LUND UNIVERSITY

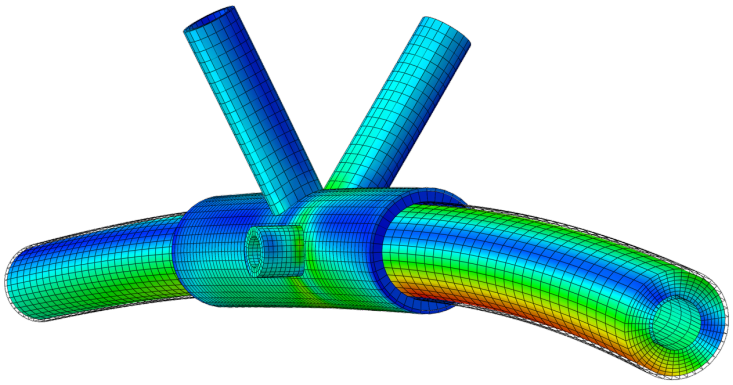

NUMERICAL ANALYSIS OF CONNECTION IN WIND TURBINE ROTOR BLADE

ALBIN INGMARSSON

Structural Mechanics

Master's Dissertation

DEPARTMENT OF CONSTRUCTION SCIENCES
DIVISION OF STRUCTURAL MECHANICS

ISRN LUTVDG/TVSM--17/5220--SE (1-68) | ISSN 0281-6679
MASTER'S DISSERTATION

NUMERICAL ANALYSIS OF CONNECTION IN WIND TURBINE ROTOR BLADE

ALBIN INGMARSSON

Supervisor: **PETER PERSSON**, PhD, Div. of Structural Mechanics, LTH.
Examiner: Professor **KENT PERSSON**, Div. of Structural Mechanics, LTH.

Printed by Media-Tryck LU, Lund, Sweden, March 2017 *(Pl)*.

For information, address:
Division of Structural Mechanics,
Faculty of Engineering LTH, Lund University, Box 118, SE-221 00 Lund, Sweden.
Homepage: www.byggmek.lth.se

Abstract

A globally growing population, an increased energy consumption and growing environmental awareness have made the interest for renewable energy sources, such as wind power, higher. As a result of the increased demand the need for new and improved technologies have increased. The energy production of a wind turbine is highly affected by the rotor blade length, which is limited by the massive dead load of the blade. Moreover, rotor blades are expensive and demanding or impossible to transport to inaccessible construction sites. These are some, among many, limitations with wind turbines, which are the premise to a new technology for rotor blades currently being developed. These, innovative wind turbine rotor blades will be longer, cheaper and more mobile than traditional rotor blades.

In a lightweight truss-like structure, e.g. the rotor blade investigated, the structural elements must be designed carefully in general and the connections in particular. One of the connections in the blade, where several of the structural elements are joint, was the focus in this project.

A number of design proposals were evaluated in numerical analyses using finite element methods. Since stress concentrations were developed in the initial design proposal a new design of the connection, where additional structural elements were introduced, was proposed. By introducing a steel pipe and a thin layer of adhesive material, the stresses were distributed more evenly and the loads were transferred more efficient. It was shown that a soft, highly deformable, adhesive is preferable. Moreover, a design of adhesive such that abrupt changes in stiffness are minimised is favourable. This can be achieved by alternating the stiffness over the lap, either by vary the thickness of the layer or by vary the properties of the material. Furthermore, the main beams of the blade should be made of carbon fibre reinforced composite with a layup that was defined.

Moreover, using the designs of the connection element that were considered feasible yet another numerical model was established. This, simplified, model was designed for a defined set up in an upcoming experimental testing. The results from this model can be combined with the results from the experimental testing for proof of concept, to validate the models and to identify sources of errors.

Keywords: Wind turbines, rotor blades, renewable energy, lightweight, truss structure, fibre reinforced composite, adhesive, finite element method.

Preface

This master dissertation concludes my Master's degree in Structural and Civil Engineering. The master's thesis was carried out for the Division of Structural Mechanics at Lund University Faculty of Engineering.

I would like to thank Dr. Peter Persson and Prof. Kent Persson for supervising me, giving me feedback and guidance throughout the work. Furthermore, I would like to send my gratitude to the co-workers at Winfoor AB for the support.

Last but by no means least; I would like to thank my family and friends for the support they gave me throughout my education.

Albin Ingmarsson
Lund, Sweden
February 2017

Contents

1 Introduction

1.1 Background

A globally growing population, political regulations, a more environmental conscious community and an increased energy consumption have made the interest for renewable sources higher. Throughout the history, a majority of the energy have been produced through fossil or nuclear sources, but a more environmental conscious population has resulted in a rapid growth in technologies for renewable energy sources, such as wind power. Since the wind turbine for electricity production took off in the 1980s the research and technology has increased significantly. In Figure 1.1 the size and power increases of commercially manufactured wind turbines between 1982 and 2006 is illustrated. Furthermore, the figure illustrates a clear relationship between the rotor blade length and the produced power.

The bending stiffness arising from the mass of the blades sets an upper limit to the blade length. Yet another factor setting the upper limit for wind turbines with the current design is transportation. Many sites are inaccessible, which makes it difficult or impossible to transport the, more than 80 meter long, rotor blades, the wide tower sections or the cranes necessary for erection of the wind turbine on site [1]. As of today rotor blades accounts for around 20% of the total cost of large wind turbines. It has been shown that, with the technology and design of today, the manufacturing cost of the wind turbine follows a relationship proportional to its mass [2].

The company 'Winfoor AB' develops a technology of wind turbine rotor blades called 'Triblade'. Figure 1.2 is a CAD-model developed by Winfoor of the blade. The Triblade aims to improve and enable production of renewable energy by designing a wind turbine rotor blade that is longer, cheaper and more mobile than traditional blades. The lightweight design and use of composite materials results in a drastic reduction of the blade mass, hence the blade can be built longer. As can be seen in Figure 1.1 there is a relationship between the blade diameter and the energy production. Moreover, the reduced weight can, because of the relationship between mass and manufacturing cost mentioned above, reduce this cost. Furthermore, the technology of Triblade is developed to be produced in a number of parts that can be assembled on site to form the full blade. This both simplifies the transportation of the blade and gives the opportunity to construct wind turbines at remote and inaccessible locations.

In a lightweight, truss-like, structure such as the Triblade, the connection elements are crucial to transfer the arising forces. Furthermore, the forces a wind turbine rotor blade is subjected to varies substantially with diverse load cases, from impulse loads

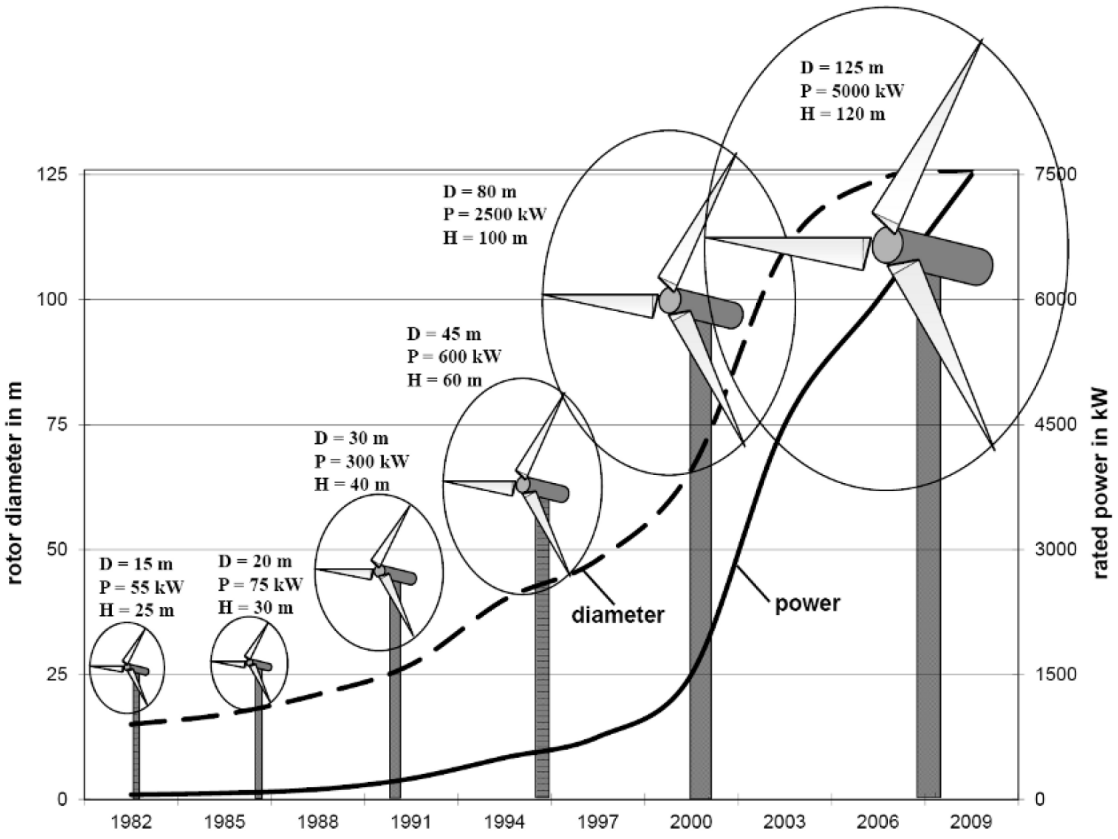

Figure 1.1: *The evolution of rotor diameter, rated power and height of wind turbines [1].*

from high wind speeds when the rotor is positioned in an unfavourable position to cyclic loads when the turbine is in service.

Previous works carried out within the Triblade technology include computational fluid dynamics (CFD) analysis of the aerodynamics [3] and structural analysis of the truss structure including non-linear analysis, dynamic response and response to impulse [4]. Moreover, a detailed analysis of the connection where the beams of the blades are joint with cohesive material has been carried out [5]. The most recent design proposal is the basis for this project, where the blade design will be investigated further with a detailed analysis of a connection element that requires special attention.

1.2 Aims and objective

The aim of this master thesis is to investigate a connection element in the Triblade and design it to transfer the arising forces in an efficient manner. The aim of the project is reached through four objectives:

- Come up with a design proposal of the connection element.
- Develop a numerical model by use of finite element method of the suggested

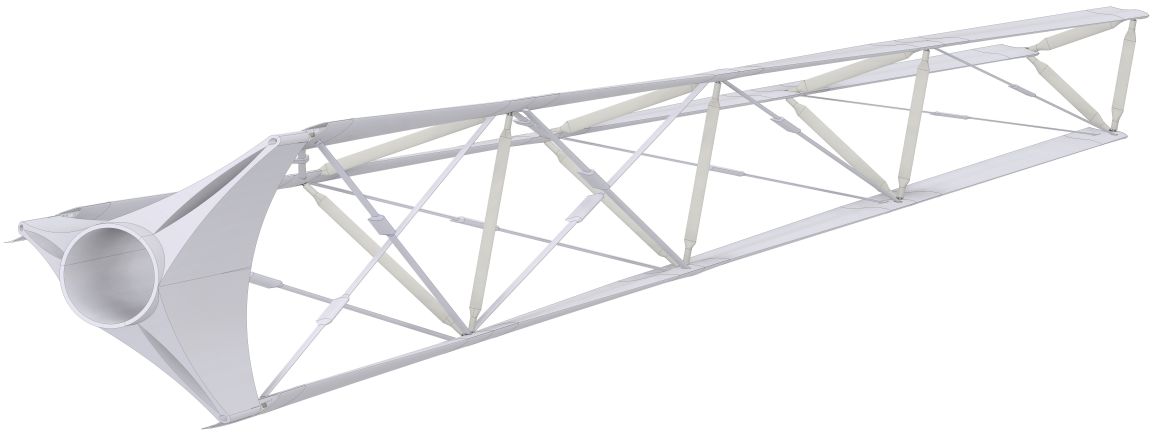

Figure 1.2: *CAD-drawing of the Triblade developed by Winfoor.*

design.

- Propose a simplified set up for experimental testing in laboratory to be carried out in the future.
- By use of finite element method develop a numerical model for the experimental testing in laboratory.

This thesis is a part of the development of the new technology for the wind turbine rotor blade called 'Triblade' by the company 'Winfoor AB'. The results and conclusions in this thesis will be used for the final design of the Triblade.

1.3 Limitations

Following limitations of the project applies:

- The connection subjected to the highest load was identified and was the connection element investigated. The design proposed for this connection is assumed to be applicable for all similar connection elements in the blade.
- The worst load case for the selected connection element was defined and all analyses were carried out in static conditions. Hence, dynamic loads and fatigue of materials were not considered and no attention was paid to other load cases.
- In the numerical analysis for experimental testing a load case with one single concentrated force was defined. Hence, not all loads the connection element is subjected to in service were considered.
- A design of the Triblade with a length of roughly 10 meters was used when the connection element was analysed. If and how the results from this model can be used for a longer Triblade was not studied.

- No experimental testing were carried out to find mechanical characteristics. Hence, the mechanical behaviour defined for the materials in the numerical analysis were supported by literature or other sources.

1.4 Outline

1 Introduction	The background, aims, objective, and limitations of the master's thesis are presented.
2 Wind turbines	Brief description of traditional wind turbine blades and the Triblade technology. Moreover, the connection element analysed and the forces acting on the element are described.
3 Materials	The materials used in the numerical analyses are described with basic theory, mechanical properties and other relevant aspects.
4 Theory	Covers theory of the methods utilised in the project. Theory explained includes the finite element method, material models and failure prediction.
5 Numerical analysis	The numerical analyses, including model descriptions, analysis results and discussions, are presented.
6 Concluding remarks	Concludes the report with conclusions from the work performed and recommendations for future work.

2 Wind turbines

2.1 Traditional rotor blades

The moving mass in the air in wind contains kinetic energy. Conversion of this kinetic energy is to mechanical energy occurs when the wind propagates rotation in the rotor blades of a wind turbine. Subsequently, conversion of mechanical energy in the rotor blades to mechanical energy occurs by use of a turbine. In the design of rotor blades, both structural factors and aerodynamic principles must be considered. The former aspect ensures both the static and dynamic forces arising in the blade can be transferred whereas the later satisfies the ambition of gathering as much energy from the wind as possible. It should be noted that both wind turbines with horizontal and vertical axis of rotation exists but it has been shown that the former design is preferable [1].

The power existing in wind can be expressed as [1]:

$$P_{wind} = \frac{1}{2}\rho A v^3, \tag{2.1}$$

where ρ is the density of the air, v is the wind velocity and A is the cross-section area perpendicular to the velocity. In other words, the power is dependent on the wind velocity to the power of three, making the choice of location of the wind turbine crucial. Furthermore, the circular rotating area formed when the rotor blades rotates makes the length of the rotor blades, i.e. the radius of the circular cross-section area, a significant factor.

When the radius of the rotor blade increases, the bending stress caused by the dead load of the blade increases. In traditional wind turbine rotor blades, this sets the upper limit for the blade length, theoretically according to following relationship:

$$m \sim R^3. \tag{2.2}$$

In Equation 2.2, m is the mass and R is the radius of the rotor blade. To increase the rotor diameter further and thus increase the power production, lightweight design of rotor blades has been developed. By implementation of lightweight design the mass of the blades follows a relationship according to

$$m \sim R^{2.2}. \tag{2.3}$$

The relationships between mass and radius for lightweight and traditional rotor blades is illustrated in Figure 2.1 [1].

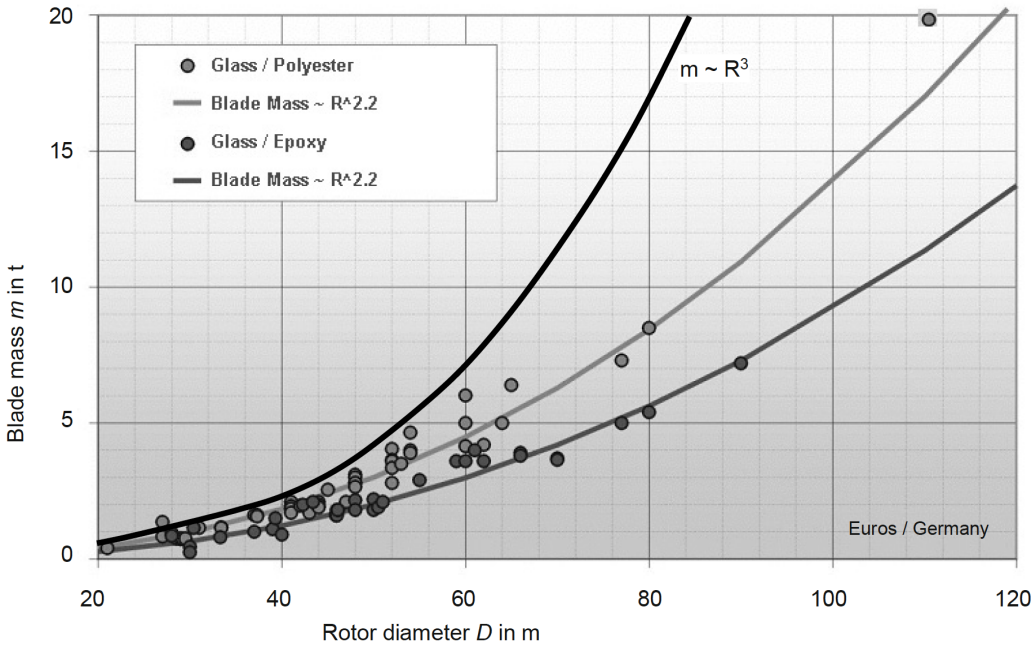

Figure 2.1: *Increase of rotor blade mass versus rotor diameter. Theoretical curve and interpolation for traditional blades ($m \sim R^3$) and light-weight blades ($m \sim R^{2.2}$) [1].*

Very rarely railways are in direct connection to the construction site of the wind turbine. Usually the, nowadays not uncommonly 80-meter long, rotor blades are transported to the construction site in one piece on trucks. The transportation and erection on site has become such a significant factor that it economically sets the limit for the use of big wind turbines in remote regions and developing countries [2].

2.2 Materials in rotor blades

Many aspects and properties must be taken into account when evaluating which material is most beneficial in a wind turbine rotor blade. Some, among many, of the most essential materials properties are [2]:

- Specific weight (kg/m^3).
- Strength limit (Pa).
- Modulus of elasticity (N/m^2).
- Fatigue strength (Pa) after millions of cycles.

In the history of wind turbines, numerous different materials have been used. In the very beginning, wood was used to build windmills but has been replaced in modern wind turbines. In the 1980's wind turbines made out of steel was the standard. Steel has suitable materials properties in terms of high stiffness and breaking length (breaking strength related to the specific weight) and the price for wind turbines made of steel is

competitive, with a relatively low material cost and low production cost. However, thick layers of steel are hard to form into a twisting shape, which is desirable to maintain good aerodynamic properties. Moreover, when using steel it is difficult to guarantee strong welding and its corrosion properties are challenging. Furthermore, the aspect making the development strive towards other materials were the fatigue strength of steel after millions of load cycles, which was the factor setting the limit for steel design. However, with the wind turbines of today in mind, the high mass of steel is reason enough to not choose it in favour for other materials, such as fibre-reinforced composites [2].

Throughout the history the research and technologies in wind turbine design has been inspired by the aerospace industry, where the search for a lightweight material with high strength drove the research for fibre-reinforced composite materials. By using fibre-reinforced composite materials in wind turbines properties such as high strength, high stiffness, and a competitive price could be combined [2].

2.3 Triblade

In Section 2.1 the relationship between electrical power production of a wind turbine and swept area was explained. Moreover, the same section covered that the stresses caused by the blades self-weight sets an upper limit of the length in traditional blades. The company 'Winfoor AB' develops 'Triblade'. The Triblade is a so called 3-1 rotor blade technology, i.e. each rotor blade contains three blades, which are connected to each other with a truss-like system as can be seen in figure Figure 2.2. The structural parts of the blade is made of lightweight materials such as fibre-reinforced composites [6].

Furthermore, as discussed in Section 2.1 the transportation and erection of the traditional heavy, solid and most importantly long blades are challenging. The Triblade technology allows the blade to be manufactured in a number of subsections that can be assembled on site. Transportation, which can be crucial for very long blades, is hence simplified and less expensive [6].

In the lightweight truss-like structure, the mass can be reduced significantly compared to the traditional rotor blades. Hence, the blades can be built longer. Moreover, up to 60% of the cost of traditional rotor blades is associated with the cost of material [6]. The Triblade aims to reduce the mass with up to 80%, reduce blade cost with 60% while it is possible to make the blades longer and the transportation and erection on site is simplified [7].

2.4 The analysed connection element

In Figure 2.2, where the major structural parts of the Triblade are illustrated, the location of the analysed connection element is shown. As can be seen in the figure the blade is principally formed by three types of structural elements: 'Blades', 'Tension rods' and 'Compression bars'. There are three blade beams in each rotor blade, which will be made of FRC with either glass or carbon fibres. To achieve good aerofoil properties a wing profile surrounds the beams, which can be seen in Figure 2.2. A

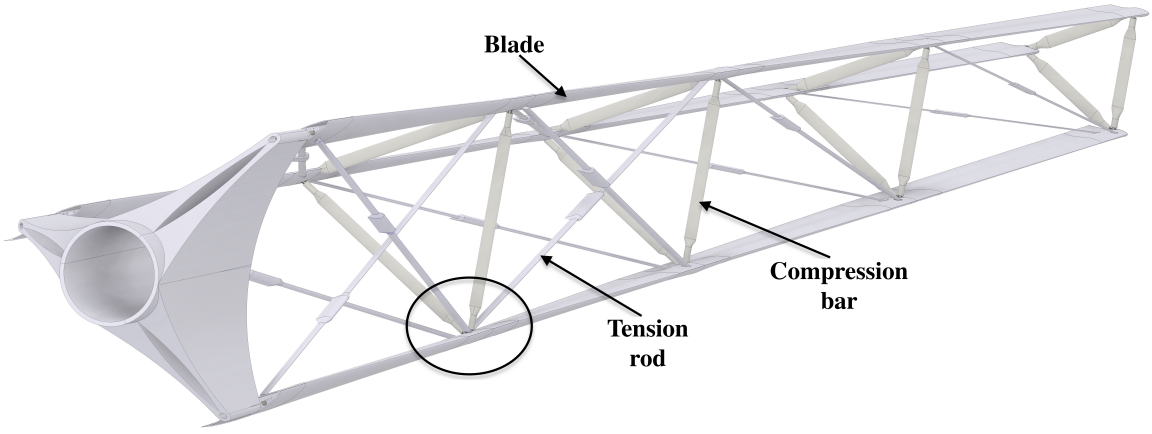

(a)

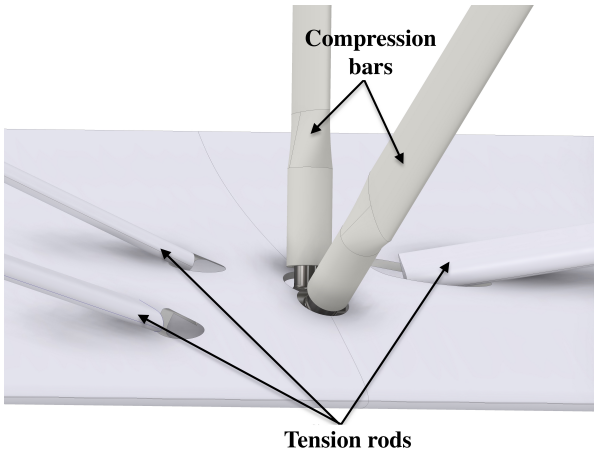

(b)

Figure 2.2: *(a) Drawing of the Triblade with labels of major elements. The connection element inside the circle is the element analysed in this project. (b) Close up drawing of the connection element analysed.*

truss-like structure is formed by connecting the beams to each other using tension rods and compression bars. The tension rods, later in this paper abbreviated 'Rods' and by Winfoor known as 'Struts', serves the purpose of transferring tension forces in the axial direction. Hence, the tension rods can be considered as ties in a structural perspective. Moreover, the compression bars, later in this paper abbreviated 'Bars' and by Winfoor known as 'Plates', transfer both forces and moments in all directions. However, the axial compression force is the dominating load in the compression bars.

At the connection, where the blade beams are joint with the tension rods and compression bars, high loads are transferred to the blade beam. Hence, these elements are considered to be critical and a detailed analyse is necessary. The connection element will be used on nine places in total in each rotor blade.

In previous work regarding Triblade, a script to calculate the internal forces for a

set length, chord length, load case and so on for the structural parts in the blade has been developed. Using the script bending moment diagrams and shear force diagrams can be generated, which aims to be used as input when designing the structural parts of the Triblade [8]. The script was developed in the script based software 'FemBem', which combines 'finite element method' (FEM) and 'blade element momentum' (BEM) theory. The basic theory of FEM is introduced in Section 4.1 and the analysis utilises the software 'CALFEM' developed by Lunds University. Using FEM structural modelling is carried out, static deformations are calculated and modal analyses are performed [9]. By combining 'blade element theory', which estimates forces in the blade generated by aerofoil effects, with 'momentum theory', which examines the balance of momentum in the turbine, the BEM theory can be formulated. By use of BEM theory the design of the blade can be optimised and performance parameters can be predicted [10]. By implementing BEM in the analysis the aerodynamics are considered and aerodynamic loads and moments in the blade are estimated. The BEM analysis was developed by Raphaël Pile and Rikard Berthilsson [9].

Using FemBem the arising forces in blade with a total length of roughly 10 meters, which is meant to be constructed as a prototype, has been calculated. The load case considered is the worst possible, i.e. a hurricane wind of 59.5 m/s and the tower oriented normal to the wind direction. The innermost connection, roughly 3 meters from the rotor hub, in the compressed beam is the highest demanded connection. The position of this connection is illustrated in Figure 2.2. In Table A.1 in Appendix A the forces in the connection element are presented [8]. The position and local coordinate systems of the forces in Table A.1 can be seen in Figure A.1 in Appendix A. The forces in the rods are oriented in the direction of the corresponding rod and the forces in the blade (i.e. Blade 2-1 and Blade 2-2 are oriented in the local coordinate system illustrated in the centre of the beam.

3 Materials

The connection element analysed in the numerical analysis is made of steel, adhesive, fibre-reinforced composite and rubber. This section aims to cover the basics and mechanical properties of each material. Steel is the subject in Section 3.1, in Section 3.2 the characteristics and other aspects of adhesive materials are covered and in Section 3.3 fibre-reinforced composites are introduced. The chapter ends with rubber in Section 3.4, which is used in the analysis for the experimental testing to be carried out in the future in laboratory.

3.1 Steel

Steel is as an alloy of iron that contains maximum approximately 2% coal and sometimes a small portion of other substances [11].

For most calculations knowing the Young's modulus, shear modulus, yield strength and ultimate strength is sufficient. In Figure 3.1, a stress-strain diagram for a typical steel is presented. In the diagram most of the material properties can be found. The Young's modulus, E, is the relationship between stress and strain in the elastic region. This can be found by the gradient in the linear elastic region to the very left in the diagram. Linear elasticity will be discussed further in Section 4.2.1. All steel materials for construction purposes are assumed to have a Young's modulus of 210 GPa. The yield strength, σ^y, is the stress when the linear elastic relationship ends and plastic strains are developed [11]. As illustrated in Figure 3.1 the plastic material behaviour of steel usually includes both a perfectly plastic region and a strain hardening region. The theory for these behaviours are covered in Section 4.2.2. The yield strength can vary from roughly 200 MPa to more than 1 GPa [12]. Depending on which structural steel is used the strain at this point, ϵ^y, is approximately 0.1–0.3%. Ultimate strength, σ^y, is the highest stress the material is subjected to before failure. Finally, the shear modulus, G, cannot be found directly through the stress-strain curve. However, for an isotropic material in the elastic region the shear modulus can be expressed as

$$G = \frac{E}{2(1+\nu)}. \tag{3.1}$$

The ratio of transverse to axial strain, Poisson's ratio, ν, is 0.3 for steel in the elastic region. The shear modulus is then 81 GPa in the elastic region [11].

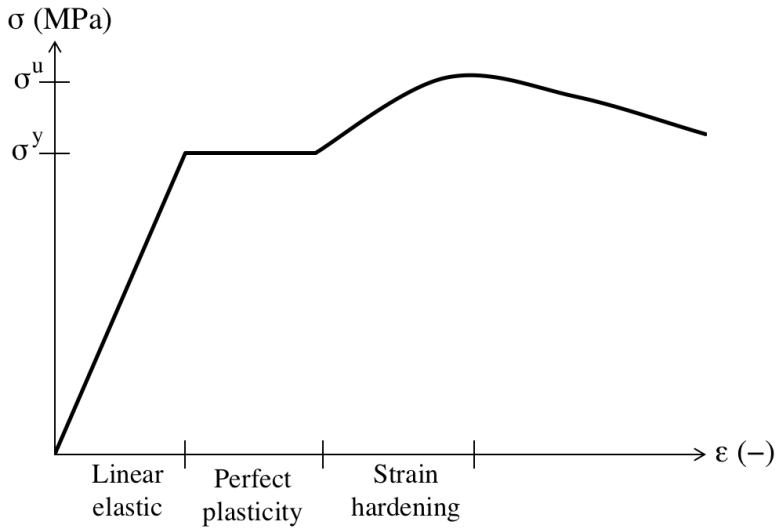

Figure 3.1: *Typical stress-strain diagram for steel.*

3.2 Adhesive

Adhesives are used to bond two surfaces, known as 'substrates' to each other through adhesion. An adhesive can either be a two-component (abbreviated as 2C) or a single-component (abbreviated as 1C) system. A 2C system consist of two different components that are mixed on site whereas a 1C system usually bonds by providing heat (heat curing system) or by providing moisture (moisture curing system) [13]. Adhesives are built up by a chemical composition containing numerous chemicals, hence there are a more or less infinite number of different adhesives on the market and an adhesive can be produced to fit the requirements for a specific application. However, the most commonly used adhesives on the market consist of epoxy, polyurethane, reactive acrylic and silicone for example. Each category can be varied in numerous ways and a mix of chemical types can build up an adhesive, thus the properties of the adhesive can be greatly varied. Moreover, the properties of an adhesive is usually modified by adding a small portion of other components to the mix [14].

3.2.1 Mechanical properties

An adhesive material is a complex material, which usually is designed to fit the specific application. As mentioned above the chemical composition and so on affects the properties of an adhesive. Moreover, the properties are often dependent on the surface and design of the joint. Hence, properly defining mechanical properties of an adhered joint without testing is very difficult. Lap shear strength (LSS), shear modulus, stress-strain relationship and durability are some among many material properties that are relevant for an adhesive material [13].

The lap strength gives an approximate value of the strength of the adhesive. However, since the substrates and geometry of the joint has a significant impact on the

strength, a lap shear strength should not be used to find the strength of a joint. By using a lap shear test according to a standard, e.g. 'DIN 53283' and 'EN 1465', the lap shear strength is measured. The test is a tensile test with substrates and adhesives set up as illustrated in Figure 3.2. The width, w, is usually 25 mm and the overlap length, b, 12.5 mm [13].

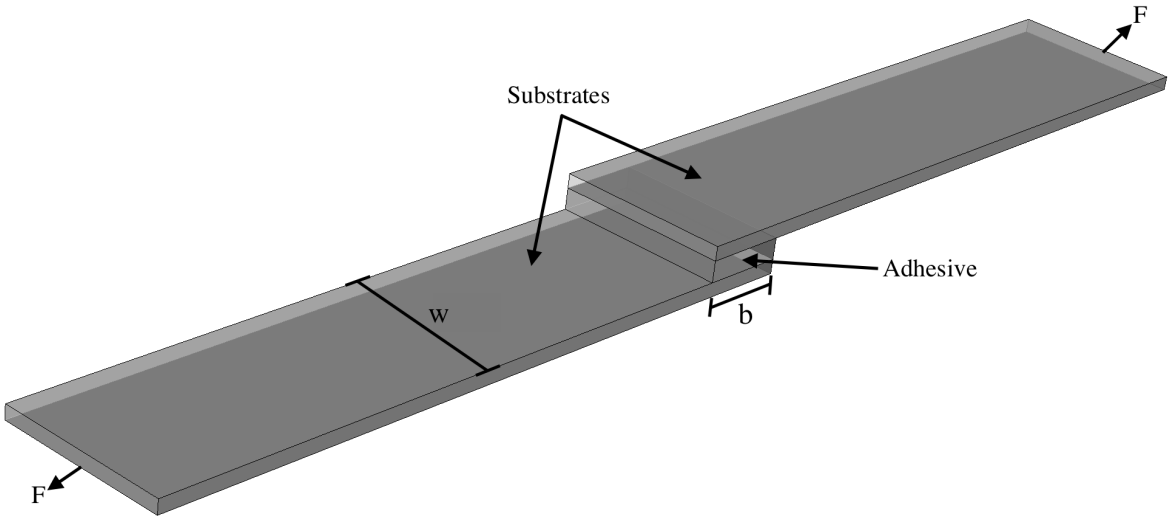

Figure 3.2: *Set up for lap shear test.*

3.2.2 Properties of selected adhesives

Two different adhesives, with significantly different characteristics, were used in the numerical analysis: the soft, highly deformable adhesive 'SikaFast-5215 NT' and the stiff epoxy adheisve '3M DP490'.

SikaFast-5215 NT

'SikaFast-5215 NT', a soft, highly deformable adhesive was analysed in the connection element. According to product data sheet the adhesive has a tensile strength, σ_{max} and shear strength, τ_{max}, of approximately 10 MPa. Furthermore, the producer provided results from three lap shear test according to the standard 'EN 1465'. According to the test, SikaFast-5215 NT has a lap shear strength of 11.37 MPa with a standard deviation of 0.39 MPa. Both product data sheet as well as results from lap shear test of the adhesive can be found in Appendix B. By the end of the project, new research regarding the mechanical properties of SikaFast-5215 NT came to light. According to the research the mechanical characteristics of SikaFast-5215 NT varies greatly depending on loading speed and temperature. Since the connection element will be subjected to permanent loads and the temperature will vary significantly the SikaFast-5215 NT was considered to be inappropriate for the connection [15]. However, since a great deal of work was put into designing the connection element with SikaFast-5215 NT before this information

came to light and the results and conclusions might be applicable for similar adhesives it is included in the report.

3M DP490

'3M DP 490', a stiff, epoxy adhesive, was also analysed in the connection element. The adhesive can be approximated using a linear elastic material model, as explained in Section 4.2.1, with the properties presented in Table 3.1 [16].

Table 3.1: *Properties for 3M DP490 [16]. In the table E is Young's modulus, G is shear modulus, ν is Poisson's ratio, σ_{max} is tensile strength and τ_{max} is shear strength.*

E (MPa)	G (MPa)	ν (–)	σ_{max} (MPa)	τ_{max} (MPa)
1,907.2	745	0.28	32	18.8

3.3 Fibre-reinforced composite

Fibre-reinforced composites (FRCs) are made up by matrix material with fibres embedded. The fibres, usually made of glass or carbon, work as reinforcement with high modulus and strength and carry a majority of the load. The matrix makes sure the fibres are oriented and located as desired, transfers load between fibres and protects the fibres from harmful environmental conditions [17]. The modulus and strength of FRCs are comparable with traditional metals, such as steel. However, because of the low density of fibre-reinforced composites the modulus and strength per unit weight is in favour for FRCs compared to traditional metals. Moreover, the properties related to fatigue are considerably better for FRCs than for traditional metals. The competitive properties per unit weight has made FRC popular in applications such as aircraft, space, and automotive. However, compared to metals, which often are considered isotropic, the properties of fibre-reinforced composites strongly depend on the direction of the fibres. The anisotropic properties of the composite are vital for achieving a suitable material but also gives an opportunity to create a unique material with properties matching the requirements for the specific application [17].

The type of fibre material and the type of matrix material used affect the properties of the composite. Different fibres will be discussed further in Section 3.3.1. The material in the matrix can for example be polymeric, metallic or ceramic. The basics of the matrix will be covered more thoroughly in Section 3.3.2. The fundamentals of laminating theory to form a FRC is the topic in Section 3.3.3 and in 3.3.4 mechanical properties of selected FRCs are presented. Lastly, in Section 3.3.5, the critical aspect to consider when joining fibre-reinforced composites are explained.

3.3.1 Fibre

The fibres are the primary load-carries in a FRC and the length, volume fraction, orientation and type of fibre determines the final properties in terms of e.g. density,

strength, modulus, fatigue strength and cost. Hence, the decisions when choosing fibre material in the composite is crucial for creating a suitable composite. The fibres typically have a circular cross-section with a diameter of 5-10 μm. Glass, carbon and aramid are example of commonly used fibre materials.

The two most common glass fibres are E-glass and S-glass. Building a composite with glass fibres has the advantages of a high tensile strength, good insulation abilities, and high chemical resistance while the cost is low. Glass fibre comes with the disadvantages of low tensile modulus, relatively low fatigue resistance and compared to other fibres relatively high density.

Numerous types of carbon fibre with different properties are available on the market. Carbon fibre has a high tensile strength and tensile modulus with respect to its low density. In addition, carbon fibre has advantages such as high fatigue strength and low coefficient of linear thermal expansion. However, using carbon as a fibre material comes with disadvantages such as high electrical conductivity and low strain-to-failure values. Furthermore, carbon fibre are more expensive than glass fibre.

Lastly, Kevlar 49 is a trade name of an aramid fibre with a low density and high tensile strength related to its weight. Composites with aramid fibres are difficult to cut and has a low compressive strength [17].

3.3.2 Matrix

The main functions of the matrix material in a FRC are to keep the fibres at desired location and orientation, protect the fibres from harmful environment and transfer forces between the embedded fibres. Even though the matrix has a minor influence on the composite's tensile capacity, it is important for its compressive strength. Polymeric, metallic and ceramic are three types of matrix material typically used, where the former is the most commonly used. Primarily metallic and ceramic matrix material are used in environments with high temperature. Hence, these are not discussed further in the thesis.

Polymeric matrix types are divided into two categories: thermoset and thermoplastic. In the former the individual molecules are chemically connected to each other, whereas weak secondary bonds keep the individual molecules in thermoplastic polymers in place. Tensile modulus, tensile strength and fracture toughness are the most significant properties of the polymer. Naturally, other properties can be relevant depending on, for example, the type of load and environment.

3.3.3 Laminating structure and design technique

Layers of fibres embedded in a matrix material form a solid section, i.e. the FRC. Varying the orientation of the fibres in the different layers, the layer thickness', the position of the layers in the layup modifies the composites properties. Moreover, whether the fibres are continuous or discontinuous affects the properties of the composite.

The numerous ways to modify the material results in a situation where the material can be constructed to fit the requirements for the unique application. The angles of the fibres affects the properties of the composite in the fibre-plane. However, since

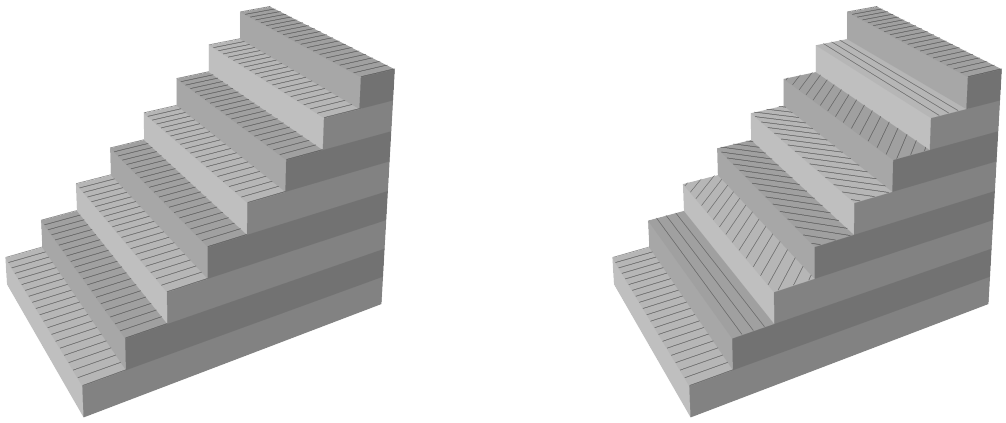

(a) (b)

Figure 3.3: *Example of composite layups with corresponding name. (a): Unidirectional (UD) layup, i.e. all fibres in one direction, [0°]. (b): Multidirectional layup, [0/90/45/-45°]$_S$.*

there are no fibres oriented in the stacking direction the orientation of the fibres will have an insignificant impact on the properties in this direction and the matrix material properties are substantial. Since the matrix is weaker than the fibres, the stacking direction will be the weakest direction.

The nomenclature to specify the layup is by the angles, θ, of each layer to a set axis in the fibre-plane. The laminate angles are presented inside square brackets and the subscript 'S' denotes a layup that is symmetric by its mid-plane [17]. In Figure 3.3 two layups with names according to the nomenclature are illustrated.

Because of the complexity of a FRC and the numerous ways to modify a FRC, there is no unambiguous method to design the layup for a complex load case. However, in general the design procedure of a composite follows three steps [17]:

1. Choose fibre and matrix material and volume fraction of each component.

2. Select layup including orientation and arrangement of fibre layers.

3. Estimate number of plies necessary in each direction.

Today the design procedure is commonly carried out using a finite element software, a numerical method discussed further in Section 4.1. Even though the design approach is the same for FRCs as for isotropic metals, the complexity that follows with the orthotropic properties results in more input data necessary. Example of input data necessary includes materials for matrix and fibres, tensile, compressive and shear modulus, layup and much more. To get an accurate result, orthotropic materials must be evaluated using different failure criterion than isotropic materials [17]. A failure criteria for fibre-reinforced composites is introduced in Section 4.3.

3.3.4 Mechanical properties

In Table 3.2 mechanical properties for one FRC made of carbon fibres and one FRC made of glass fibres are presented. The properties presented are for unidirectional composites with 60 volumetric percent fibres in dry conditions and in room temperature. The manufacturer of the specimen for experimental testing estimated the produced composite elements to consist of approximately 72 volumetric percent fibres.

Table 3.2: *Mechanical properties of one unidirectional FRC made of carbon fibres and one made of glass fibres [18].*

	Carbon FRC	Glass FRC
Young's modulus 0°, E_1 (GPa)	135	40
Young's modulus 90°, E_2 (GPa)	10	8
Poisson's ratio, ν_{12} (–)	0.3	0.25
In-plane shear modulus, G_{12} (GPa)	5	4
Tensile stress fibre direction, X_t (MPa)	1,500	1,000
Compressive stress fibre direction, X_c (MPa)	1,200	600
Tensile stress transverse direction, Y_t (MPa)	50	30
Compressive stress transverse direction, Y_c (MPa)	250	110
Shear strength, S (MPa)	50	40

3.3.5 Joining fibre-reinforced composites

Since a situation where the loads are transferred in an efficient manner is desirable a connection between two load-bearing elements must be investigated thoroughly. When a material plasticitates the stresses distributes over a bigger volume, which reduces the maximum stress in the region. However, since fibre-reinforced composites do not have a mechanical behaviour that includes plasticity a connection between an element of FRC and another element is significantly crucial. Moreover, the area surrounding the joint is normally the weakest area in a structure of fibre-reinforced composites [17].

Techniques for joining FRC elements can be divided into two categories: mechanical and bonded joints. Normally used techniques as mechanical joints are bolting or rivets whereas using a layer of an adhesive material is a bonded joining technique. Advantages with the former technique includes easy assembling, disassembling and inspecting and requires little surface preparation. Disadvantages with mechanical joints includes added weight, risk for stress concentrations and necessary to make holes in the elements, an interference that weakens the element.

The later technique, bonded joint, distributes the load over a bigger area and does not add weight or require holes. However, surface preparation is necessary, inspection and disassemble is difficult and the adhesive material may be affected by environmental conditions [17]. In a bonded joint, it can be challenging to introduce the loads to the fibres in the FRC smoothly. A method to better transfer the loads to a bigger portion of the cross-section is by designing the joint as a scarf joint [19]. Moreover, it is beneficial to design the FRC with fibres parallel to the loading direction in the surface layers [17].

It is desirable to design the components to achieve equal factor elasticity modulus, E, times thickness, h (i.e. $E_1h_1 = E_2h_2$) when a bonded joining technique is utilised [17]. Furthermore, an appropriate adhesive for this area of application has high shear and tensile strength and low shear and tensile modulus. Using an adhesive with low modulus and low strength near the ends of the lap and an adhesive with higher modulus and high strength in the central regions of the lap, can be reduce stress concentrations at the end of the lap. The adhesive with high modulus will carry more load than the adhesive with low modulus, resulting in a more even stress distribution and enhanced bearing capacity [17, 19].

Bonded joining technique can be combined with mechanical joining technique in a joint with a fibre reinforced composites and another component. Embedding a number of elements in the FRC can increase the mechanical performance of the joint. By embedding these protrusion before the FRC has cured the fibres are kept continuous and surrounds the protrusions [19].

3.4 Rubber

Naturally occurring rubber materials have been used for centuries and hundreds of years ago latex was dried to achieve an elastic, flexible, tough and water resistant material. In the late 1830's vulcanisation, i.e. create links between rubber and sulfur by applying heat, was discovered. Vulcanisation improves properties of the rubber such as tensile strength, stiffness and hardness. Roughly one century later, in the 1940's synthetic rubbers had been found and it was discovered that a polymer with special, rubber-like, properties could be vulcanised by mixing it with a small portion of isoprene [20].

Rubbers today are made of numerous components to form a material with properties corresponding to the ones desired for the specific application. The compounding process includes choice of elastomer, filler and chemicals for crosslinking and additives. Commonly used rubber materials include natural rubber (NR), styrene-butadiene rubber (SBR), polybutadiene rubber (BR), neoprene (CR) and butyl rubber (IIR).

In the analysis for the planned experimental testing in laboratory rubber material were used to decrease the, otherwise high, stresses developed at the attachments. The rubber was modelled with the hyperelastic material model 'Neo-Hookean', which is introduced in Section 4.2.3. In the model the C_{10}-coefficient was set to 1 MPa and the D_1-coefficient was not prescribed. In the experimental testing in laboratory, which will be carried out in the future, a rubber with these characteristics will be used.

4 Theory

In this, section the theory used in the project is presented. The numerical method utilised in the analysis, finite element (FE) method, is the topic in Section 4.1. Material models, used to mathematically predict how the material will behave, are covered in Section 4.2. Lastly, in Section 4.3, the theory of the used failure criterion, which forecast when the material will fail, are presented.

4.1 The finite element method

The purpose of this section is to introduce the theory of the FE method. The concept and the formulation of FEM is explained in Section 4.1.1. Explained in Section 4.1.2 are the theory of the different element types.

4.1.1 The formulation

The FE method is a numerical approximate method of solving differential equations. The basic concept is to divide the region to be analysed into smaller parts known as 'finite elements'. Subsequently an approximate solution for these finite elements are found. Because of the smaller parts, using a simple approximation method in each element is possible to find an approximate solution. When an approximation has been found for each finite element the approximations can be added together to establish a solution for the whole region. The collection of finite elements that represents the whole region is known as the 'finite element mesh'.

The FE method can be expressed in the general form presented in Equation 4.1, where the constitutive behaviour of the region is described by the stiffness matrix, $\mathbf{K}$. Furthermore, $\mathbf{a}$ is a vector containing known and unknown degrees of freedom. Finally, $\mathbf{f}$ is a vector containing known external forces as well as unknown internal forces [21].

$$\mathbf{Ka} = \mathbf{f} \tag{4.1}$$

It can be shown that to obtain a unique solution to Equation 4.1 system presented above a number of degree of freedoms must to be prescribed, i.e. the physical quantity in a number of nodes must be known. The FE method is applicable to diverse fields of application, e.g. groundwater flow, diffusion, heat conduction and elastic behaviour of bodies. However, the basic form of the FE method presented in Equation 4.1 is valid for all types of static problems.

4.1.2 Finite element types

As discussed in Section 4.1.1 the region of interest is divided into a number of small element when the finite element method is utilised. There are numerous different types of elements and their behaviour can be characterised by family, degree of freedom, number of nodes, formulation and integration [22]. Presented in Figure 4.1 are a selected number of element families. The degree of freedom are the variables considered and calculated in the analysis. Hence, the degree of freedom differs depending on type of problem and element type. The mathematical theory used to describe the behaviour of the element is represented by the element formulation. Lagrangian and Eulerian are two common formulations. In most stress-displacement analyses the Lagrangian formulation is used, later in this section this formulation is discussed further [22]. Yet another formulation, hybrid formulation, which is used to deal with incompressible or nearly incompressible elements, are discussed more thoroughly in the end of this section. Finally, the approximation in the element are dependent on the numerical integration techniques used. In most cases Gaussian quadrature technique, a numerical technique to evaluate the definite integral at each nodal point, is used. Other techniques to evaluate the integral includes full or reduced integration [22].

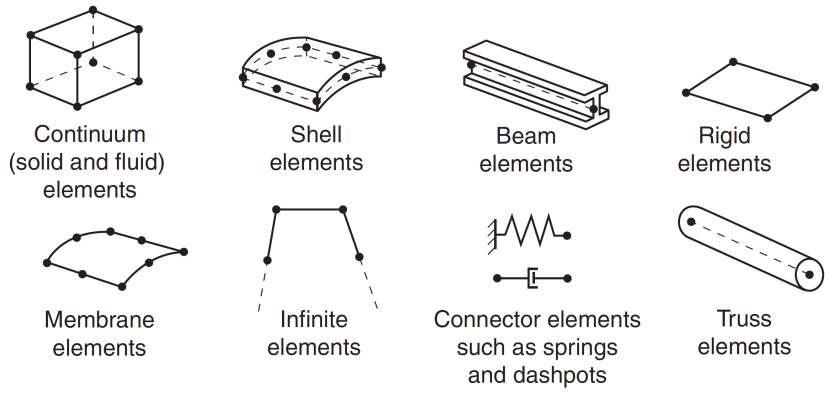

Figure 4.1: *Element families commonly used in the FE software 'Abaqus' [22].*

Continuum elements

The standard type of volume element is continuum (solid) elements, which can be used for both linear and non-linear analysis. It is possible to use continuum elements can for various applications including heat transfer, acoustics and stress. Depending on geometry and number of nodes both linear or quadratic interpolation and either full or reduced integration can be used for continuum elements. Solid elements can be one-, two- or three-dimensional with a big range of different geometries and number of nodes [22].

Shell elements

If one dimension of the geometry is significantly smaller than the others (e.g. for plates) it can be beneficial to use shell elements. Shell elements are divided into two groups:

conventional shell and continuum shell. The differences between conventional shell and continuum shell elements are illustrated in Figure 4.2. Conventional shell elements have both displacement and rotational degrees of freedom and the body is discretised in a two dimensional plane. Continuum shell elements only have displacement degrees of freedom and are discretised in three-dimensions. As with solid elements shell elements can be varied greatly, e.g. with different geometry and number of nodes [22].

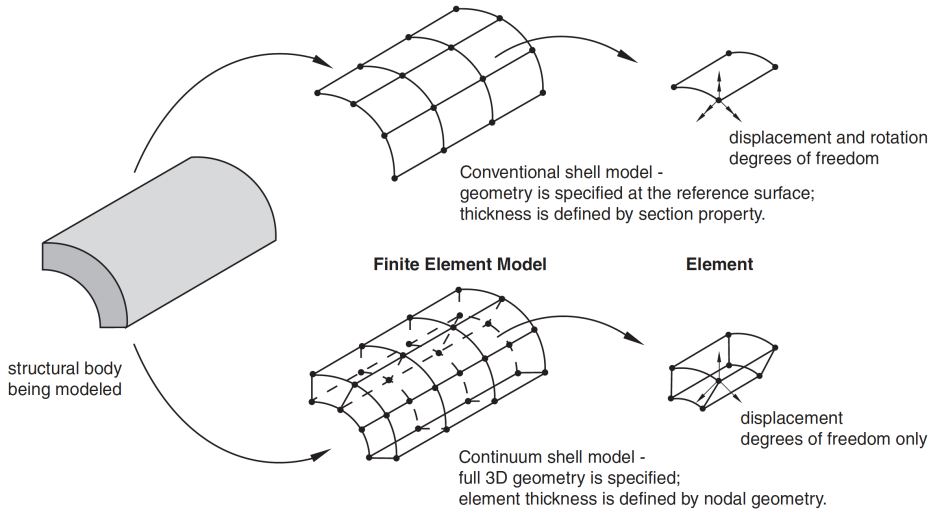

Figure 4.2: *Difference between conventional shell and continuum shell elements [22].*

Lagrangian formulation

In Lagrangian formulation the node in each element is fixed to the element. When the material deforms the element deforms and the nodes and element boundary follows this deformation. Hence, the entire element is always filled with material in Lagrangian formulation in contrast to Eulerian formulation, where the element is fixed in space and material is allowed to flow thorough the element [22].

Hybrid formulation

If an element is or is almost incompressible, it is not possible to find a solution by only using the displacement history. A material may be considered incompressible if the bulk modulus is much greater than the shear modulus or Poisson's ratio is close to 0.5. An example of a material that may be considered incompressible and hence evaluated using hybrid formulation is 'rubber'. Subjecting an incompressible material to a small displacement produces a large change in pressure. Hence, only consider displacement to find a solution is too sensitive for numerical analyses. By evaluating the pressure independently, removes this sensitivity in hybrid formulation, hence it is also known as 'mixed formulation'. Using Lagrange multiplier the pressure can be linked to the displacement through constitutive relationships and compatibility conditions. It should also be noted that many materials show incompressible behaviour at large strains even if they do not at small stains [22].

4.2 Material models

In Section 3 the materials used in the numerical model and experimental testing where introduced. When a material is subjected to stresses a mathematical material model is utilised in the numerical analysis to predict how it will react and behave. These material models are the focus in this section. In Section 4.2.1 the simplest model, linear elasticity, is briefly explained followed by plasticity in Section 4.2.2. The subject in Section 4.2.3 are hyperelastic material models.

4.2.1 Linear elastic

The simplest material model is the linear elastic. The term 'elastic' means that the deformation are reversible and the term 'linear' refers to a linear relationship between the stress, σ, and strain, ϵ. This relationship can be described by Hooke's law [23]:

$$\sigma = E\epsilon, \tag{4.2}$$

where E is the modulus of elasticity, also known as Young's modulus. Moreover, if the material is assumed isotropic the relationship between stress and strain in three dimensions can be expressed as:

$$\begin{bmatrix} \varepsilon_{11} \\ \epsilon_{22} \\ \epsilon_{33} \\ \gamma_{13} \\ \gamma_{13} \\ \gamma_{23} \end{bmatrix} = \begin{bmatrix} 1/E & -\nu/E & -\nu/E & 0 & 0 & 0 \\ -\nu/E & 1/E & -\nu/E & 0 & 0 & 0 \\ -\nu/E & -\nu/E & 1/E & 0 & 0 & 0 \\ 0 & 0 & 0 & 1/G & 0 & 0 \\ 0 & 0 & 0 & 0 & 1/G & 0 \\ 0 & 0 & 0 & 0 & 0 & 1/G \end{bmatrix} \begin{bmatrix} \sigma_{11} \\ \sigma_{22} \\ \sigma_{33} \\ \sigma_{13} \\ \sigma_{13} \\ \sigma_{23} \end{bmatrix}, \tag{4.3}$$

where E is the Young's modulus, ν is the Poisson's ratio, G is the shear modulus, σ are the stresses, ϵ are the strains and γ are the shear strains. The subscript following the strains and stresses denotes to the direction [22]. In the equation it can easily be seen that the stress-strain relationship in each direction is linear, which is illustrated in Figure 4.3.

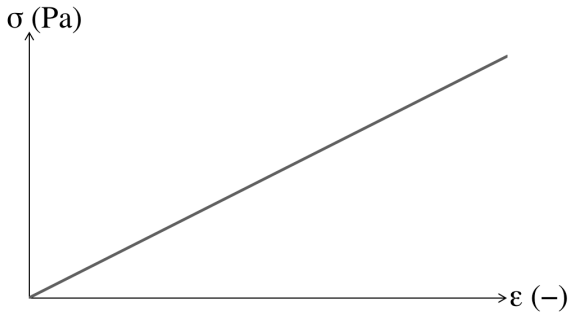

Figure 4.3: *Stress-strain relationship according to the linear elastic material model.*

Moreover, according to Hooke's law following relationships applies [24]:

$$G = \frac{E}{2(1+\nu)} \tag{4.4}$$

$$K = \frac{E}{3(1-2\nu)}, \tag{4.5}$$

where Equation 4.5 K is the bulk modulus. By use of Equation 4.4, Equation 4.3 can be expressed with only the Young's modulus and Poisson's ratio as unknowns.

4.2.2 Plasticity

When the stresses are high the strains developed in some materials, e.g. steel, becomes irreversible. These irreversible strains are known as 'plastic strains'. Plasticity can be evaluated using a function of stress and strain known as the yield function, f. The total strain in a material model including elastic and plastic behaviour is the sum of the elastic strain, ϵ^e, and the plastic strain, ϵ^p [24]:

$$\epsilon = \epsilon^e + \epsilon^p. \tag{4.6}$$

Two material models including plasticity were used in the numerical analysis: 'elastic perfectly-plastic' and 'linear elastic-plastic'. The remaining of this section briefly introduces these two material models.

Elastic perfectly-plastic

If an elastic perfectly-plastic material model is used the stress-strain relationship is elastic and linear until the yield stress, σ^y, is reached and the material begins to plasticise. When the yield stress has been reached the plastic strains increases even though the stress is constant. The stress-strain behaviour of an elastic perfectly-plastic material is illustrated in Figure 4.4 [24].

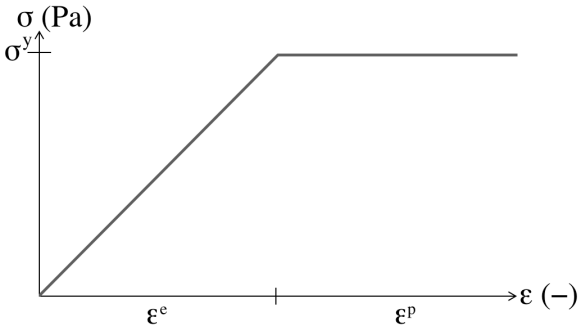

Figure 4.4: *Stress-strain relationship according to the elastic perfectly-plastic material model.*

Linear elastic-plastic

Similarly to elastic perfectly-plastic material model the stress-strain relationship is elastic and linear until the yield stress, σ^y, is reached in the linear elastic-plastic material model. However, in the linear elastic-plastic material model the stresses increases in the plastic region. This behaviour in the plastic region, where the stresses increases while plastic strains are developed is known as 'strain hardening'. The gradient in the plastic region is less than the gradient in the in the elastic region. A typical stress-strain relationship according to the linear elastic-plastic is illustrated in Figure 4.5 [23].

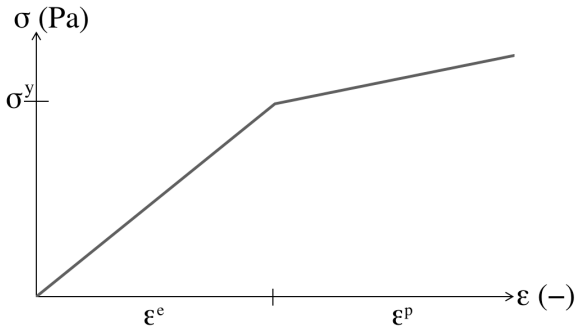

Figure 4.5: *Stress-strain relationship according to the linear elastic-plastic material model.*

4.2.3 Hyperelastic material

The hyperelastic material model assumes the material to be isotropic and nonlinear and to deform elastic even at large strains. As mentioned in Section 3.4, rubbers are formed by elastomer that typically can be assumed incompressible, i.e. the volume does not change when subjected to stresses. Furthermore, a consequence from the low compressibility is a Poisson's ratio close to 0.5 [22].

The deviatoric strain invariants of order i, $\bar{I}_i$, can be used to formulate the strain energy potential, U, of a hyperelastic material. The polynomial form of strain energy is expressed as [22]

$$U = \sum_{i+j=1}^{N} C_{ij}(\bar{I}_1 - 3)^i(\bar{I}_2 - 3)^j + \sum_{i=1}^{N} \frac{1}{D_i}(J^{el} - 1)^{2i}, \tag{4.7}$$

where N is a material dependent parameter, C_{ij} and D_i are material parameters dependent on the temperature. Moreover, J^{el} is the elastic volume ratio, which is the factor between the total volume ratio, J, and the thermal volume ratio J^{th}, i.e.

$$J^{el} = \frac{J}{J^{th}}. \tag{4.8}$$

The initial shear modulus, μ_0, and bulk modulus, K_0, can be expressed in terms of the parameters C_{10}, C_{01} and D_1:

$$\mu_0 = 2(C_{10} + C_{01}), \tag{4.9}$$

$$K_0 = \frac{2}{D_1}. \tag{4.10}$$

By making special assumption of C_{ij}, the Neo-Hookean form can expressed

$$U = C_{10}(\bar{I}_1 - 3) + \frac{1}{D_1}(J^{el} - 1)^2. \tag{4.11}$$

With similar definitions of the parameters as for Equation 4.7. Equation 4.10 still applies. However, the shear modulus, μ_0, is found using Equation 4.12 [22].

$$\mu_0 = 2C_{10}. \tag{4.12}$$

4.3 Material failure criteria

The theory of von Mises, a failure prediction typically used for isotropic materials such as steel is presented in Section 4.3.1. Section 4.3.2 covers the theory of Tsai-Hill failure criterion, which can be used for composite materials. Presented in Section 4.3.3 are material failure in adhesive bonds.

4.3.1 von Mises

In Section 4.2.1 and Section 4.2.2 the basics of elasticity and plasticity were introduced, respectively. To determine the stresses and evaluate whether materials with a plastic behaviour will yield when subjected to loading, the von Mises stress is typically used. The von Mises stress combines the stress distribution from normal and shear stresses in a three dimensional solid to one scalar [25]. Subsequently, comparing the scaler with the yield and ultimate strength for the isotropic material.

The von Mises stress can be expressed as [25]

$$\sigma_{vM} = \sqrt{\frac{1}{2}\left[\Big(\sigma_{xx} - \sigma yy\Big)^2 + \Big(\sigma_{yy} - \sigma zz\Big)^2 + \Big(\sigma_{zz} - \sigma_{xx}\Big)^2\right] + 3\Big(\tau_{xy}^2 + \tau_{yz}^2 + \tau_{zx}^2\Big)}, \tag{4.13}$$

where the subscripts x, y and z denotes three orthogonal directions, σ is normal stresses and τ shear stresses.

4.3.2 Tsai-Hill

The von Mises failure criterion presented above is commonly used when designing isotropic materials against yielding. Since fibre-reinforced composites neither are designed for yielding nor are isotopic materials, other criterion must be used to achieve trustworthy and accurate results [17]. A failure criteria commonly used when observing a single laminate is the Tsai-Hill criterion. The Tsai-Hill criterion allows interaction between multi-axial stresses to define the strength in the five failure modes, i.e. longitudinal and transverse tension, longitudinal and transverse compression and shear. The

Tsai-Hill criterion was derived by implementing anisotropic properties and strength parameter of a lamina into the von Mises criterion [26]. The Tsai-Hill criteria is expressed as [22]:

$$\left(\frac{\sigma_{11}}{X}\right)^2 - \frac{\sigma_{11}\sigma_{22}}{X^2} + \left(\frac{\sigma_{11}}{X}\right)^2 + \left(\frac{\sigma_{12}}{S}\right)^2 < 1.0. \tag{4.14}$$

In Equation 4.14, σ_{11}, σ_{22} and σ_{12} are longitudinal, transverse and shear stresses, respectively. Moreover, X and Y are tensile and compressive strength in longitudinal and transverse direction, respectively. Finally, S is shear strength in the 1-2 plane.

If the value on the left-hand side of the equation exceeds 1.0 the stresses leads to failure in the lamina. Similarly, if the value on the left-hand side is lower than 1.0 failure will not occur.

4.3.3 Failure in adhesive bonds

An adhesive material is usually used to connect two surfaces, known as adherends, to each other. The failure in an adhesive bond can be divided into three categories [27]:

- Cohesion failure, i.e. fracture in the adhesive layer.
- The interaction between the adhesive and the adherends breaks, known as 'adhesion failure'.
- In one of the adherends, not in connection to the bond itself.

Since the later means that the adhesive joint did not break and the failure occurred in the material of one of the adherends this type of failure is desirable. The former failure, cohesion failure, is usually caused by shear stresses and results in fracture of the adhesive. Cohesion failure can also be propagated by peel stresses, i.e. the adhesive fails by stresses in the direction perpendicular to the surface of one of the adhereneds. Furthermore, cohesion failure can be caused by a combination of shear and peel stresses. Adhesion failure occurs when the interaction between the surface of one the adherends and the adhesive is not strong enough, which typically is caused by hydration of the chemical bonds between the two surfaces. In general, adhesion failure in service is a consequence of the manufacturing process, e.g. bonding was not formed before curing and the surface was not chemically active.

5 Numerical analysis

Different designs of the connection element were proposed. To evaluate and make necessary modifications of the design to make it transfer the forces arising in an efficient manner, numerical analyses were conducted. Initially, each design proposal was evaluated with a simplified numerical model in a so-called feasibility study. If the results from the simplified analysis were considered feasible, the proposal was investigated further with a gradually more accurate and detailed analysis.

The outline of this section and is as follows:

- Design proposal I, i.e. the design of the connection element that has been used in previous development of the Triblade, is covered in Section 5.1.
  - A simplified model, used to make a feasibility study is presented in Section 5.1.1.
  - Results from the analysis of the simplified model are presented in Section 5.1.2.
  - The results from Section 5.1.2 are discussed in Section 5.1.3.
- Design proposal II, a design proposal with additional structural elements introduced, is presented in Section 5.2.
  - Since an adhesive layer was introduced an analysis to find the material characteristics of a soft adhesive was carried out, which is presented in Section 5.2.1. Furthermore, since the characteristics of the fibre-reinforced composite (FRC) was defined in more detailed in this design proposal an analysis to find the most beneficial layup of the FRC was carried out. The methods and results from this analysis are also covered in Section 5.2.1.
  - A numerical analysis aimed to represent the rotor blade in service, i.e. taking the whole geometry, all loads into account, was conducted. This is presented in Section 5.2.2.
  - Section 5.2.3 covers the numerical analysis and model used to determine a simplified set up for the upcoming experimental testing.
  - In Section 5.2.4 the results from Section 5.2.2 and Section 5.2.3 are presented.
  - The results presented in Section 5.2.4 are discussed in Section 5.2.5.

5.1 Design proposal I

In the design proposal, the blade beam made of fibre-reinforced composite, is constructed joint with the compression bars connecting the three beams in one part. This is illustrated in Figure 5.1. To fit into the wing profile designed in previous works, the upper limit of the blade beam's diameter was set to 38 mm. By varying the blade beam's diameter, between 30 mm and 38 mm, and the wall-thickness, between 3 mm and 6 mm, potential effects on the results is found. Rod-connections made of steel connects the tension rods with the beams. The rod-connections has the shape of a cylinder, which is continuous and pears through the blade beam. The rod-connections' diameter was set to 16 mm and the length to 65 mm.

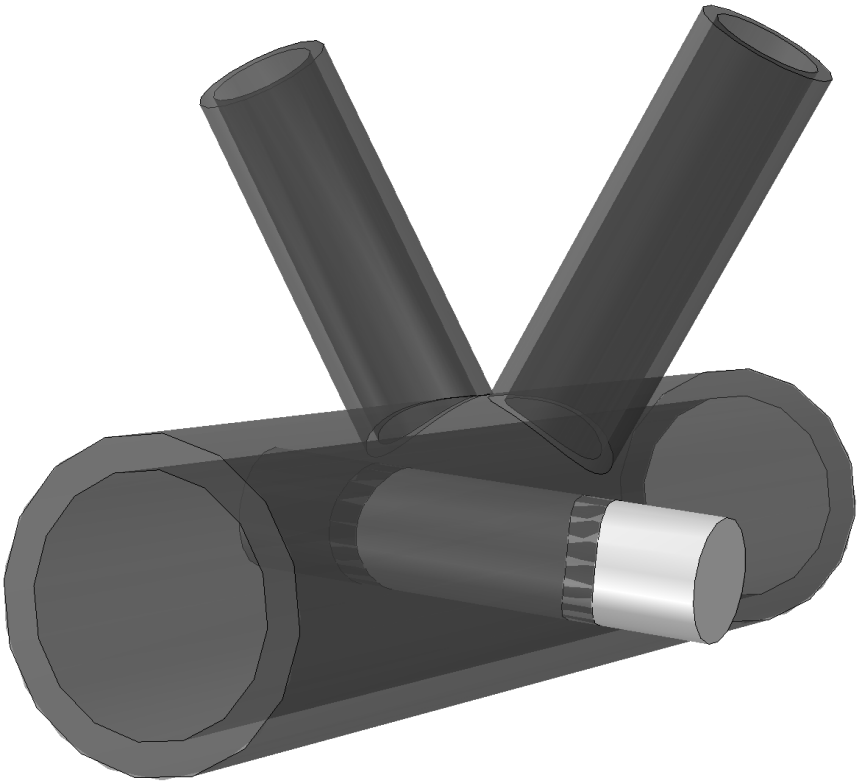

Figure 5.1: *Illustration of design proposal for connection element. The sections in transparent black (blade beam and compression bars) are made of FRC and the grey cylinder (rod-connection) is made of steel.*

The steel in the rod-connection is much stiffer than the FRC in the blade beam. As discussed in Section 3.3.5 a connection between two materials with varying stiffness normally results in stress concentrations where the stiffness decreases. Hence, the region where the rod-connection is connected to the blade beam was defined as the critical region.

5.1.1 Model for feasibility study

The model of the design that was established to perform an initial numerical analysis of the connection is illustrated in Figure 5.2. The impact from the compression bars is considered to be negligible for the stress distribution around the area where the rod-connection and blade beam are joint. Hence, the compression bars are not included in the model used in the feasibility analysis. The model is simplified further by only including the rod-connection subjected to the highest loads. The blade beam is 163.2 mm long and, as mentioned previously, the wall thickness was varied between 3 mm and 6 mm and the diameter was varied between 30 mm and 38 mm.

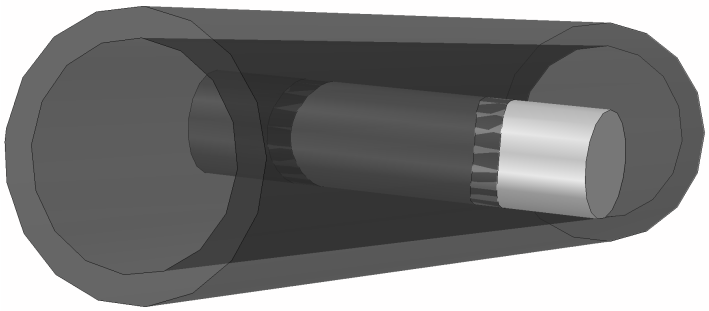

Figure 5.2: *Model for feasibility study of initial design proposal. The blade beam, in transparent black, is made of FRC and the rod-connection, in grey, is made of steel.*

Material properties

Steel, which the rod-connection is made of, was assumed to behave according to an elastic perfectly-plastic material model as explained in Section 4.2.2. Following this assumption, the Young's modulus, Poisson's ratio and the yield strength was assumed to be 210 GPa, 0.3 and 400 MPa, respectively. To simplify the calculations during the initial analysis, an isotropic linear elastic material model, which was introduced in Section 4.2.1 was used for the fibre-reinforced composite material. The assumed properties being a Young's modulus of 70 GPa and a Poisson's ratio of 0.3.

Load case

As shown in Section 2.4, the connection is subjected to several different loads applied at different locations of the element. However, in the initial analysis, where only the joint between the rod-connection and blade beam is analysed, the forces from the compression rods were defined as the most significant. Hence, only the normal tension force in 'Tension rod 1' and 'Tension rod 6', as illustrated and presented in Figure A.1 and Table A.1 respectively, were considered. Since the tension rods will be constructed as ties (i.e. can only transfer tension forces in axial direction) a concentrated force on each rod-connection was used. The load case was simplified further by applying the average force from the two compression rods on each side of the rod-connection.

Interactions, constraints and boundary conditions

The surfaces on the rod-connection and the blade beam was connected using a frictional interaction. A tangential behaviour with a friction coefficient of 0.15 was defined.

In Figure 5.3, a multiple-point constraint (MPC) that was defined at the two ends of the blade beam, is illustrated. The control point of the MPC was defined in the centre of the cross-section and all nodes on cross-section area were defined as slave nodes. A MPC is a way to define a constraint between degrees of freedom in the model. In this analysis both the displacement and rotational degrees of freedom was constrained, i.e. a MPC of type 'Beam' in Abaqus was used [22].

The two control points in the MPCs were allocated boundary conditions, one fixed and the other was prescribed in displacement along X and Y axis and rotation around Z axis according to the coordinate system defined in Figure 5.3.

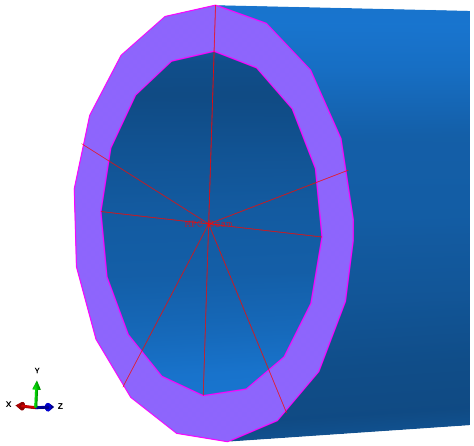

Figure 5.3: *The MPC, illustrated in red, was defined at both ends of the blade beam.*

Mesh

Since the behaviour in the region surrounding the rod-connection was of special interest, the mesh was finer in this region. The mesh for the whole assembly is illustrated in Figure 5.4. All elements are 3D continuum hexahedral elements with linear approximation and reduced integration was used. In the cylindrical rod-connection structured meshing technique was used. Similarly, structured meshing technique was used in the areas that are not in contact with the hole in the blade beam. The region in the beam surrounding the hole for the rod-connection was meshed using sweep technique.

5.1.2 Results

In Figure 5.5, the von Mises stresses in the assembly and in area surrounding the hole in the beam are illustrated for a design of the blade beam with an outer diameter of 38 mm and wall thickness of 4 mm. In the figure, the stress concentration in the area surrounding the hole in the beam for the rod-connection can be seen.

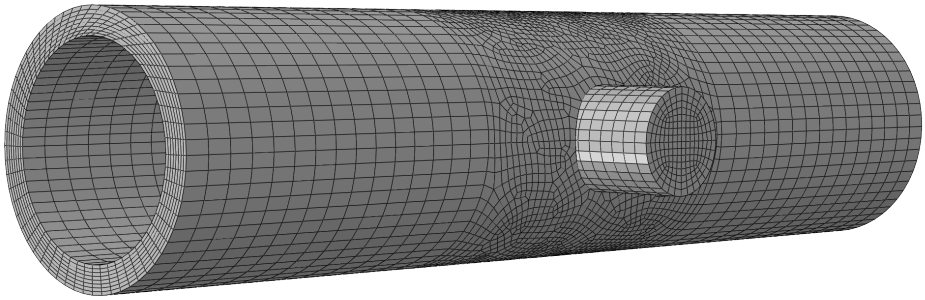

Figure 5.4: *The mesh used in feasibility study.*

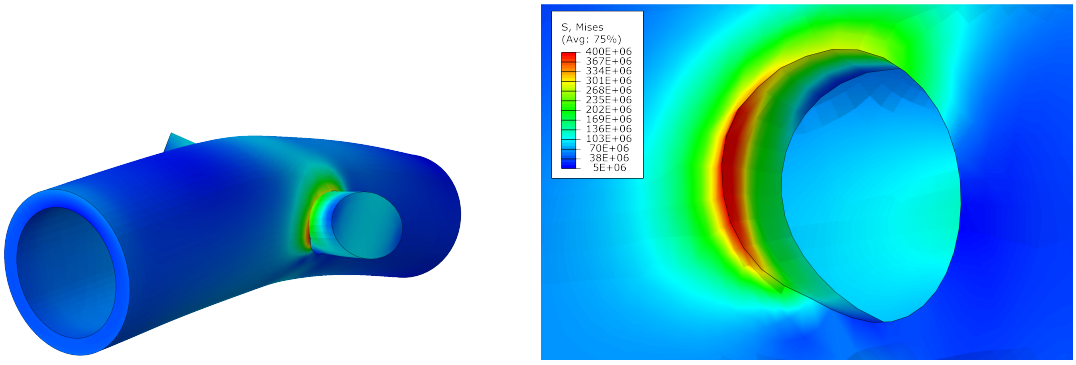

(a) (b)

Figure 5.5: *Distribution of von Mises stresses in the composite beam for a design of the blade beam with an outer diameter of 38 mm and wall thickness of 4 mm. (a) Complete assembly. (b) Blade beam in the region surrounding the cavity for the rod-connection.*

5.1.3 Discussion of results

As can be seen in Figure 5.5, a stress concentration occurs in the blade beam in the area surrounding the hole for the rod-connection. Since the stiffness is drastically reduced where the steel, with a relatively high Young's modulus, are joint with the composite, with a relatively low Young's modulus, this stress concentration is expected. In the attempt to make the stress distribution less concentrated, the diameter and wall thickness of the composite was varied. Since this had little to no effect on the stress distribution, the proposed design was discarded.

5.2 Design proposal II

Since Design proposal I was shown to not be feasible, a new design was suggested. In the proposal a steel pipe, as illustrated in Figure 5.6, was introduced. The compression bars and rod-connections are welded to the steel section. The blade beam fits inside the

steel pipe. The purpose of introducing the steel section is to be able to distribute the loads from the compression bars and rod-connections to the blade beam over a larger area. Moreover, the rod-connections and compression bars can be joint to the steel section through welding, which simplifies these connections significantly.

In Figure 5.6 the geometry of the steel section with the rod-connections and compression bars is illustrated. To fit into the wing profile, the upper limit of the outer diameter for the connection was set to 38 mm. The dimensions, shapes and materials of the components were varied to find what parameters had a considerable effect on the results. Moreover, since sudden drop in stiffness results in stress concentrations, a thin layer of adhesive material was introduced between the steel section and the blade beam. In Section 5.2.1 the numerical analysis and the results to estimate the properties of the soft, deformable, adhesive used in the connection element are presented. When the models gradually were made more accurate and detailed the characteristics of the FRC had to be determined more precise. The analyses performed in the investigation established to determine the most beneficial layup for the fibre reinforced composite in the blade beam are covered in Section 5.2.1.

In Section 5.2.2 a model which aims to represent reality, i.e. with the whole geometry, realistic load case and boundary conditions is presented. The model for a simplified set up, which will be used in an upcoming experimental testing in laboratory, is presented in Section 5.2.3. In Section 5.2.4 the results from Section 5.2.2 and Section 5.2.3 are presented. These results are discussed in Section 5.2.5.

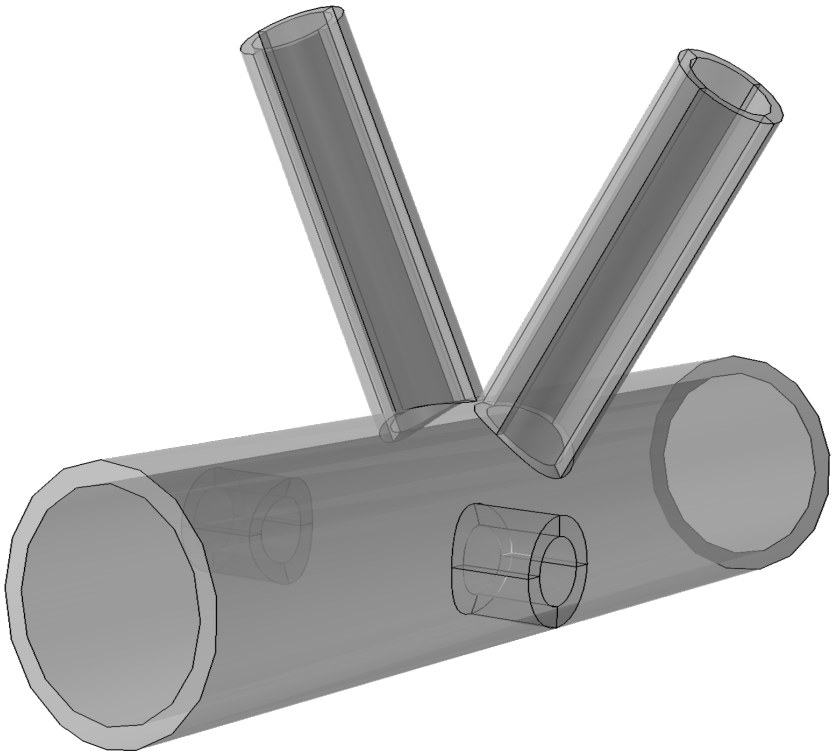

Figure 5.6: *Geometry of the steel section. The rod-connections and compression bars are welded to the steel pipe.*

5.2.1 Study if characteristics of adhesive and layup of FRC

Mechanical characteristics of soft adhesive

'SikaFast-5215 NT', a soft, deformable adhesive, was introduced in Section 3.2.1. Results from lap shear tests, as described in 3.2.1 that the producer provided for the adhesive are presented in Appendix B. By conducting numerical analyses of the test material characteristics and behaviour of the adhesive could be determined.

The geometry of the model is shown in Figure 5.7, which corresponds to the standard 'EN 1465' and the experimental test. In the model the substrates are made of steel with a linear elastic material behaviour, which was introduced in Section 4.2.1. The steel was assumed to have a Young's modulus of 210 GPa and Poisson's ratio of 0.3. The width of the substrates, w, is 25 mm and the substrates were assumed to have a thickness of 2 mm. The adhesive was assumed to have a thickness of 3 mm and a width corresponding to the substrates, i.e. 25 mm. The overlap length, b, was 11.7 mm.

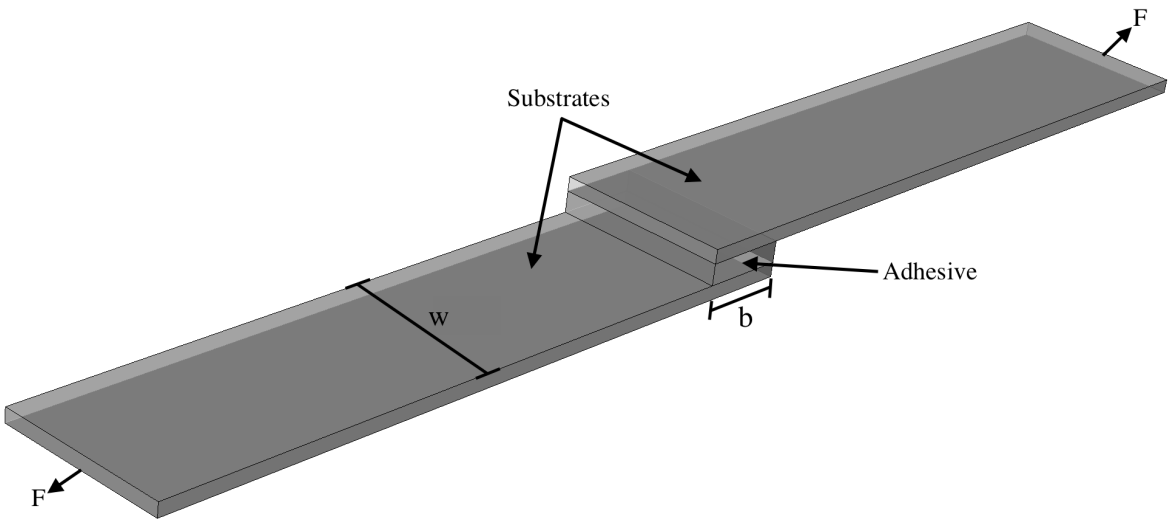

Figure 5.7: *Geometry of the lap shear test used in the numerical analyse.*

Tie constraints were defined at the surfaces connecting the adhesive to the two substrates. Linearly increasing displacements of the two edges of the substrates facing out, i.e. the two edges with the arrows labelled F in Figure 5.7, were defined. The displacements were defined in the direction of the corresponding arrow. To find the stress, the reacting force, F, was divided by the cross-section area. The stress was plotted against the displacement. Subsequently, the stress-displacement plot could be compared with the one from the physical testing presented in Appendix B.

In Figure 5.8 the material model fitting best is presented. The behaviour is characterised by an linear elastic-plastic material model with a Young's modulus of 6.5 MPa and an assumed Poisson's ratio of 0.48. The data for the plastic hardening behaviour is presented in Table 5.1.

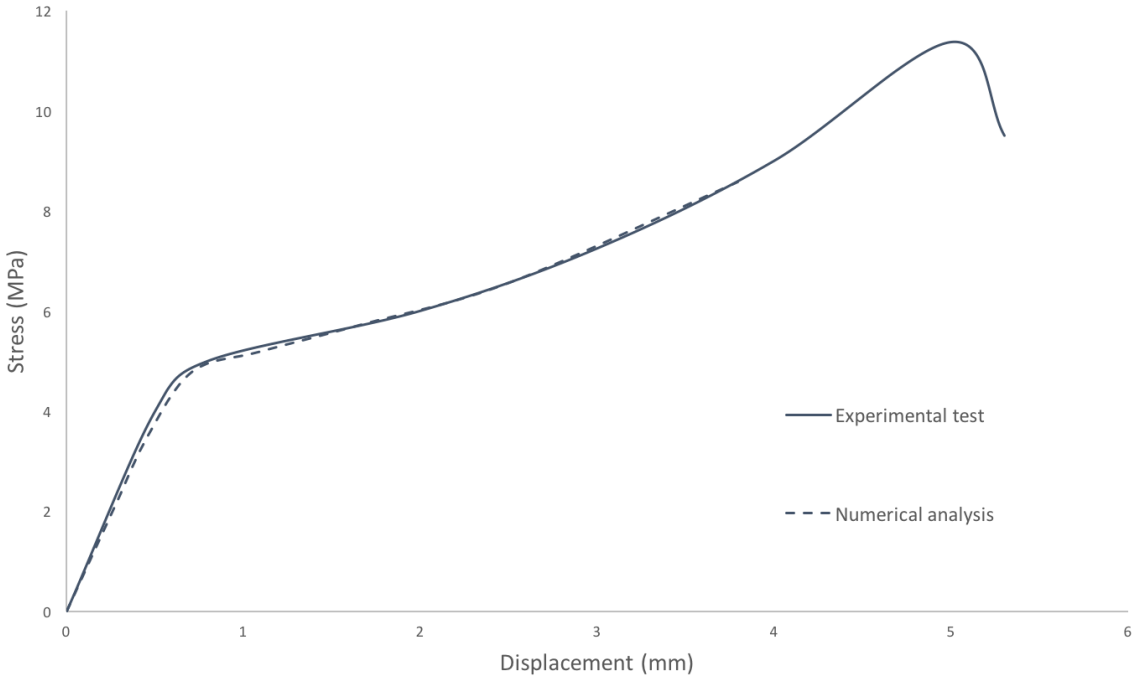

Figure 5.8: *Results from lap shear test performed in laboratory and in numerical analysis.*

Layup of fibre reinforced composite

As illustrated in Figure 5.9, the cross-section of the beam was divided into eight sections with equal wall thickness. A composite layup with 1^{th} and 2^{nd} direction in axial and tangential direction, respectively, was defined. Consequently, the stacking direction, i.e. the weakest direction, of the composite is in the radial direction of the circular beam.

The FRC was partly designed according to the design procedure presented in Section 3.3.3. In the analysis to find the most beneficial layup for the FRC in the blade beam a FRC made of carbon fibres was evaluated. A lamina was assumed to have the properties of a unidirectional composite. Hence, the material properties presented in

Table 5.1: *Plastic behaviour of SikaFast-5215 NT.*

Yield stress, f_y (MPa)	Plastic strain, ϵ_p (–)
1.4	0
2.0	0.50
2.5	0.65
3.2	0.75
10	0.85

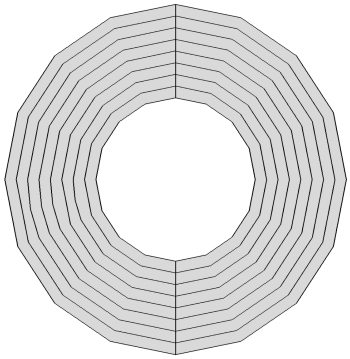

Figure 5.9: *The cross-section of the blade beam was divided into eight parts with equal thickness.*

Table 3.2 can be used to define elastic properties and failure properties for a lamina made of carbon fibres. The out-plane shear modulus's, i.e. G_{13} and G_{23}, were assumed to be equal to the in-plane shear modulus, G_{12}. The thickness Poisson's ratio and thickness modulus when defining a composite layup of continuum shell elements in Abaqus were used, i.e. thickness Poisson's ratio of 0.5 and thickness modulus equal to twice the in-plane shear modulus [22].

The composite layup was created by assigning each of the eight regions of the cross-section properties of the lamina and a rotation angle. The layup was evaluated using different combinations of angles of the fibres in the eight regions. The fibres where oriented either oriented in the axial direction of the beam, i.e. 0°, in the tangential direction of the beam, i.e. 90° or in the ±45°-directions. Moreover, the most favourable layup was found by running simulations with the fibres in different orientations stacked differently, i.e. varying position in the cross-section of the rotations. To make the analysis even more detailed, layers with different angles where created within each of the eight regions of the cross-section.

The results from the simulations is that the most beneficial layup for the FRC with carbon fibres is with approximately the innermost 10 volumetric percent of the fibres in the ±45°-direction. The remaining 90 volumetric percent of the fibres are oriented in the axial direction of the beam, i.e 0°.

5.2.2 Model for rotor blade in service

A model used to analyse the connection for a case where the rotor blade is in service was established. The model includes all parts of the connection and both the load case and boundary conditions defined aimed to represent when the rotor blade is in service.

Model

In Figure 5.10 the geometry of the assembly is illustrated. Numerous parameters, such as material properties, dimensions and shape of the components in the model were varied to investigate which parameters had a considerable effect on the results.

The blade beam is subjected to highest loads in the regions in connection to the connection element. To achieve an even utilisation rate over the length of the beam a design with a varying outer diameter and wall thickness over the length of the beam was suggested. In the drawings created by Winfoor, which are presented in Appendix C, a design of the blade beam with varying cross-section is found. For the models where the cross-section of the blade beam is constant the bigger outer diameter was used over the full length of the beam.

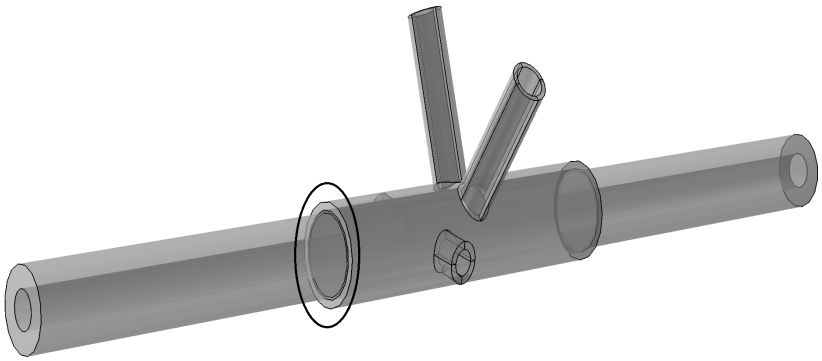

Figure 5.10: *Geometry of the assembly. The region inside the circle is the region to be tested in the laboratory.*

Material properties

All parts made of steel (i.e. the circular steel section introduced, rod-connections and compression bars) are modelled with an elastic perfectly-plastic material model. The steel has a Young's modulus and Poisson's ratio of 210 GPa and 0.3, respectively. Moreover, the parameters used to define the linear elastic-plastic behaviour are presented in Table 5.2.

Table 5.2: *Plastic behaviour of steel.*

Yield stress, f_y (MPa)	Plastic strain, ϵ_p (–)
400	0
500	0.24

The blade beam was evaluated using both a FRC made of carbon fibres and glass fibres. The material properties presented in Table 3.2 were used to define both elastic properties and failure properties for a lamina made of carbon fibres and glass fibres. The most beneficial layup was evaluated in Section 5.2.1 and was used for the FRC made of carbon fibres as well as the FRC made of glass fibres.

Since the choice of adhesive was shown to significantly affect the results, numerous different were used in the model to find a suitable material. The material characteristics of a soft, deformable adhesive were estimated in Section 5.2.1. A stiff epoxy adhesive with material characteristics presented in Table 3.1 was evaluated as well.

Furthermore, as mentioned in Section 3.3.5, a design with a stiff adhesive in the central regions of the overlap and a softer adhesive close to the end of the overlap has been shown to be beneficial to distribute the stresses more evenly and increase the load bearing capacity. Hence, a design of the layer with the quarters of the adhesive closest to the ends made of the soft adhesive and the rest made of the stiff adhesive was evaluated. This design of the adhesive is illustrated in Figure 5.11.

By varying the thickness of the adhesive, i.e. making the adhesive thicker in the ends than in the central regions of the overlap, similar characteristics were assumed to be achieved. Hence, a design where the thickness of the adhesive layer is varied over the length of the overlap was suggested. The varying thickness of the adhesive layer was achieved by linearly increasing the inner diameter of the steel section, as is illustrated in Figure 5.11.

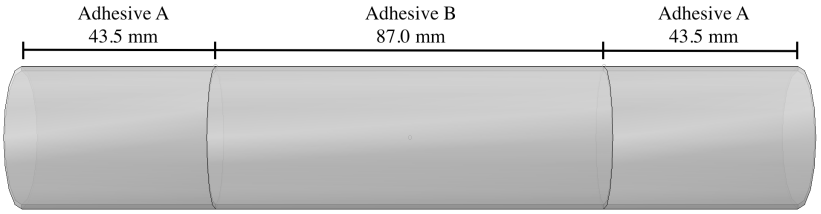

(a)

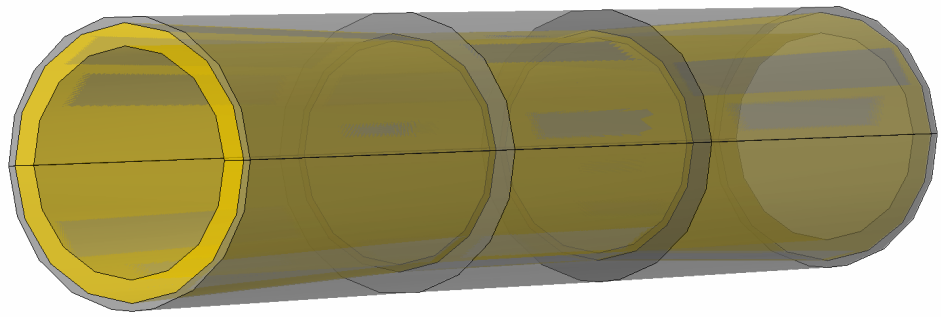

(b)

Figure 5.11: *(a) Illustration of design of adhesive layer with different types over the length. (b) Illustration of design of adhesive layer and steel section with varying wall thickness over the length. The steel is coloured in transparent grey and the adhesive in yellow.*

Constraints and boundary conditions

MPCs of type 'Beam' were used at all cross-sections facing out, i.e. at 'Blade 2-1', 'Blade 2-2', 'Rod 1', 'Rod 6', 'Bar 2-1' and 'Bar 2-2' as illustrated in Figure A.1 in Appendix A. All displacements and rotations were prescribed at the control point at the centre of the beam located at 'Blade 2-1'. Tie constraints were used to model the welding between the steel section and the rod-connections as well as between the steel section and compression bars.

Load case

All forces and moments presented in Table A.1, with positions and orientations according to Figure A.1 in Appendix A, were considered. The forces and moments were assumed to act on the control point of the MPCs.

Mesh

All parts were meshed using structured technique with hexagonal elements and linear interpolation. All elements, except the blade beam, were continuum 3D stress elements and reduced integration was used. Continuum shell elements, as explained in Section 4.1.2, were used to model the composite blade beam. Moreover, since the adhesive used has a high Poissons's, i.e. is almost incompressible, hybrid formulation was used for the adhesive. The mesh of the assembly can be seen in Figure 5.12.

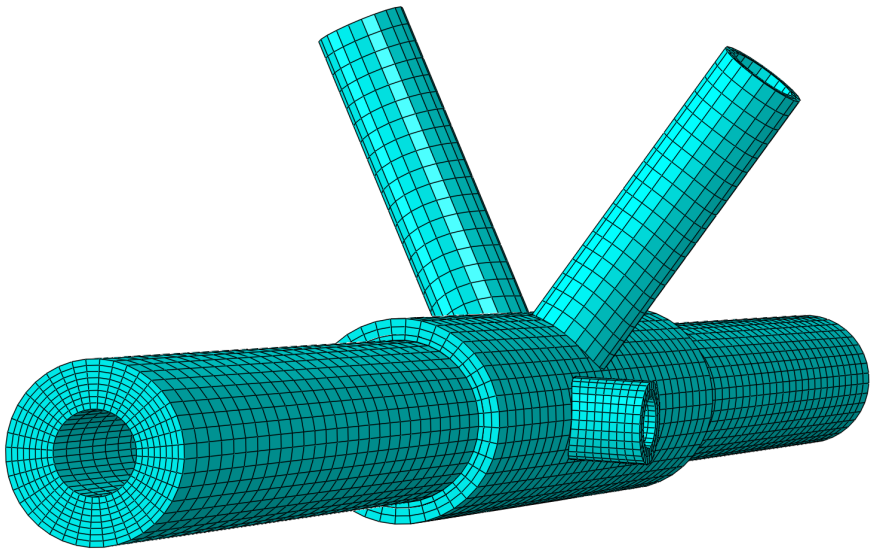

Figure 5.12: *The mesh used in the numerical analysis.*

Overview of suggested designs

An overview of the suggested models are presented in Table 5.3. The different parameters and how they are varied in the models were described in earlier text.

5.2.3 Model for experimental testing in laboratory

Similarly to Design proposal I presented in Section 5.1, the connection between the steel and FRC was defined as a critical area. This region is illustrated in Figure 5.10. Since high loads from the tension rods and compression bars must be transferred to the blade beam, this region will be investigated further through experimental testing in laboratory, which will be carried out in the future. A numerical analysis for the upcoming testing is presented in this section. The analysis was used when determining

Table 5.3: *Overview of models for rotor blade in service. The outer diameter of the blade beam and adhesive layer is either constant or varying over the length, which is given by the columns 'Beam ϕ' and 'Adhesive ϕ' respectively. 'FRC' and 'Adhesive' gives the materials in the FRC and adhesive, respectively.*

Name	Beam ϕ	FRC	Adhesive ϕ	Adhesive type
Model 1	Constant	Carbon	Constant	Stiff
Model 2	Constant	Carbon	Constant	Soft
Model 3	Constant	Carbon	Constant	Soft & stiff
Model 4	Constant	Carbon	Varying	Stiff
Model 5	Varying	Carbon	Constant	Stiff
Model 6	Constant	Glass	Constant	Stiff

the set up for the testing and can, when the testing has been carried out, be used to validate the models, identify sources of errors and for proof of concept.

Model

The presence of the rod-connections and compression bars were assumed to have a negligible influence on the forces transferred between the steel section and blade beam, hence these elements were not included in the model. Moreover, the length of the blade beam was set to 1 070 mm and the length of the steel section and adhesive was set to 170 mm. The diameter of the steel section was set to 40 mm and the wall thickness to 4 mm. Besides these changes the geometry of the model presented in Section 5.2.2 was kept intact. The geometry of the model is illustrated in Figure 5.13. To even out the stress concentration arising at the boundaries and to accommodate for physical testing in the laboratory, special attention was paid to the ends. A steel part with the shape of a circular segment was created, which can be seen in Figure 5.13. A soft (i.e. low modulus) rubber material served to reduce possible stress concentrations and was placed on the inside of the circular steel segment. The blade beam was put on top of the rubber material.

Material properties

Identical material properties to the ones presented for the model for the rotor blade in service were used for the adhesive and FRCs. The load case, with a concentrated force on the steel section, resulted in high stresses and strains in the steel. Since the purpose of the experimental test was not to test the steel section, the quality of the steel was increased. The steel was modelled according to the elastic perfectly-plastic material model introduced in 4.2.2 with Young's modulus, Poisson's ratio and yield strength of 210 GPa, 0.3 and 600 MPa, respectively. As mentioned in Section 3.4, the

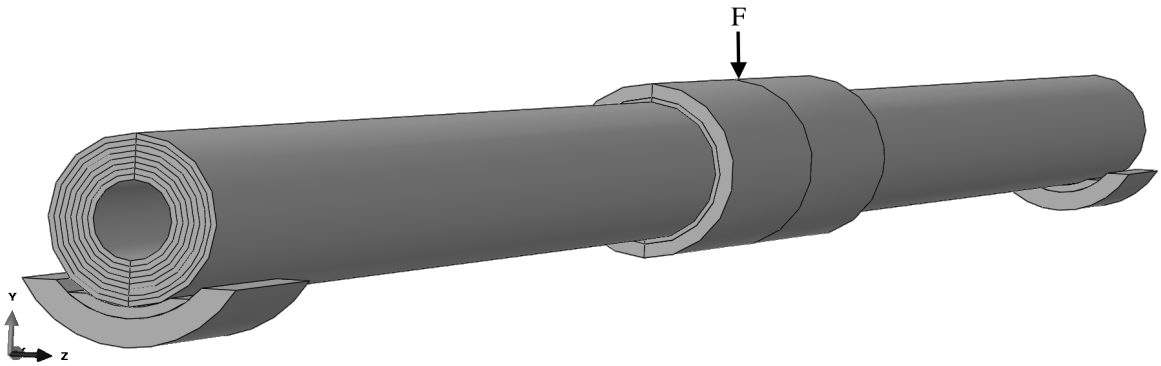

Figure 5.13: *Model for the experimental testing to be performed in a laboratory.*

rubber material was modelled using the hyperelastic model 'Neo-Hookean', covered in Section 4.2.3. C_{10} was assumed to be 1 MPa and D_1 was not prescribed.

Constraint and boundary conditions

A visual illustration of the constraints are illustrated in Figure 5.14. Tie constrains were defined on both sides of the rubber (i.e. between the rubber and the steel segment and the rubber and blade beam). Moreover, a MPC of type 'Beam' was defined on the outer surface of the steel segments. In the MPCs all nodes on the outer surface were defined as slave nodes and the nodes in the middle of the outer surface was defined as control points. The displacements and rotations around the Y- and Z-axis were prescribed to zero at the control points of the MPCs.

Load case

As illustrated in Figure 5.13 a concentrated force acting in the middle of the outer surface of the steel section was defined. The force, which is a simplified load from the compression bars, acts parallel to the Y-axis according to the coordinate system in Figure 5.13. The load is increased linearly until failure occurs.

Mesh

All parts, other than the rubber, was meshed using structural meshing technique to form a mesh of hexagonal elements. The section made of rubber is meshed using free meshing technique to form a mesh of tetrahedral elements. Short of the blade beam made of composite material, all elements are linear, continuum, 3D and reduced integration was used. For the blade beam reduced integration was used and the elements are linear from the element family 'continuum shell'. As mentioned in Section 4.1.2 hybrid formulation are used for hyperelastic materials and materials with a high Poisson's ratio. Hence, this formulation was used for the rubber and adhesive material. The mesh is illustrated in Figure 5.15.

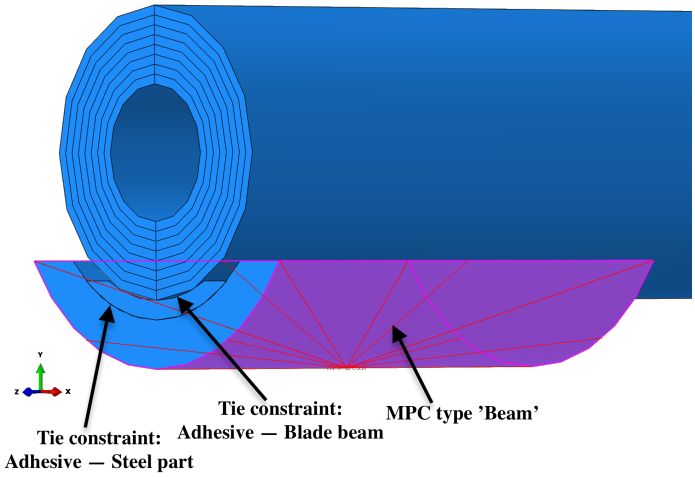

Figure 5.14: *Illustration of the constraints defined at both ends of the blade beam. The control point of the MPC was allocated boundary condition with zero displacements and rotations around the Y and Z axis.*

Overview of suggested designs

An overview of the suggested models are presented in Table 5.4. The different parameters and how they are varied in the models were described in Section 5.2.2.

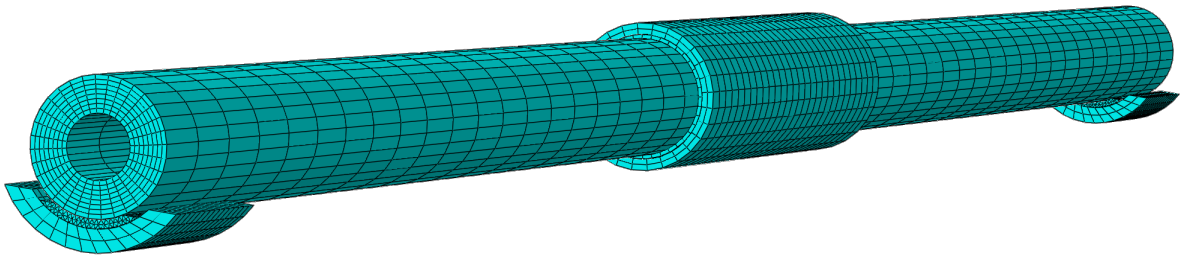

Figure 5.15: *Illustration of mesh used in numerical analysis.*

Table 5.4: *Overview of models for experimental testing. The outer diameter of the blade beam and adhesive layer is either constant or varying over the length, which is given by the columns 'Beam ϕ' and 'Adhesive ϕ' respectively. 'FRC' and 'Adhesive' gives the materials in the FRC and adhesive, respectively.*

Name	Beam ϕ	FRC	Adhesive ϕ	Adhesive type
Model 7	Constant	Carbon	Constant	Stiff
Model 8	Constant	Carbon	Varying	Stiff
Model 9	Constant	Glass	Constant	Stiff
Model 10	Constant	Glass	Varying	Stiff

5.2.4 Results

In this section the results from the numerical analyses are presented. Initially results from the models in Table 5.3, i.e. the models for rotor blade in service, are presented. Results from the models for experimental testing in laboratory, listed in Table 5.4, are presented.

Rotor blade in service

In Figure 5.16 example of results are presented. The results presented in the figure are for analysis carried out with Model 4. To systematically compare the results, a distribution of the Tsai-Hill criterion and von Mises stress along the length of the blade beam and adhesive layer, respectively, was constructed. Figure 5.17 gives an illustration, with position on the circumference and direction, of the paths, which was defined to compare the results in the blade beam and the adhesive layer. In Figure 5.18 the distribution of Tsai-Hill criterion in the path in the blade beam is illustrated. Furthermore, Figure 5.19 illustrates the distribution of the von Mises stress in the path in the adhesive. Model 6 is not included in the figures above. Since Model 6, with FRC made of glass fibres, experience higher strains and the numerical analysis fails before the loads has reached 100% it is not included in the figures. In Figure 5.20 results extracted when the loads are 50% of their total magnitude are presented.

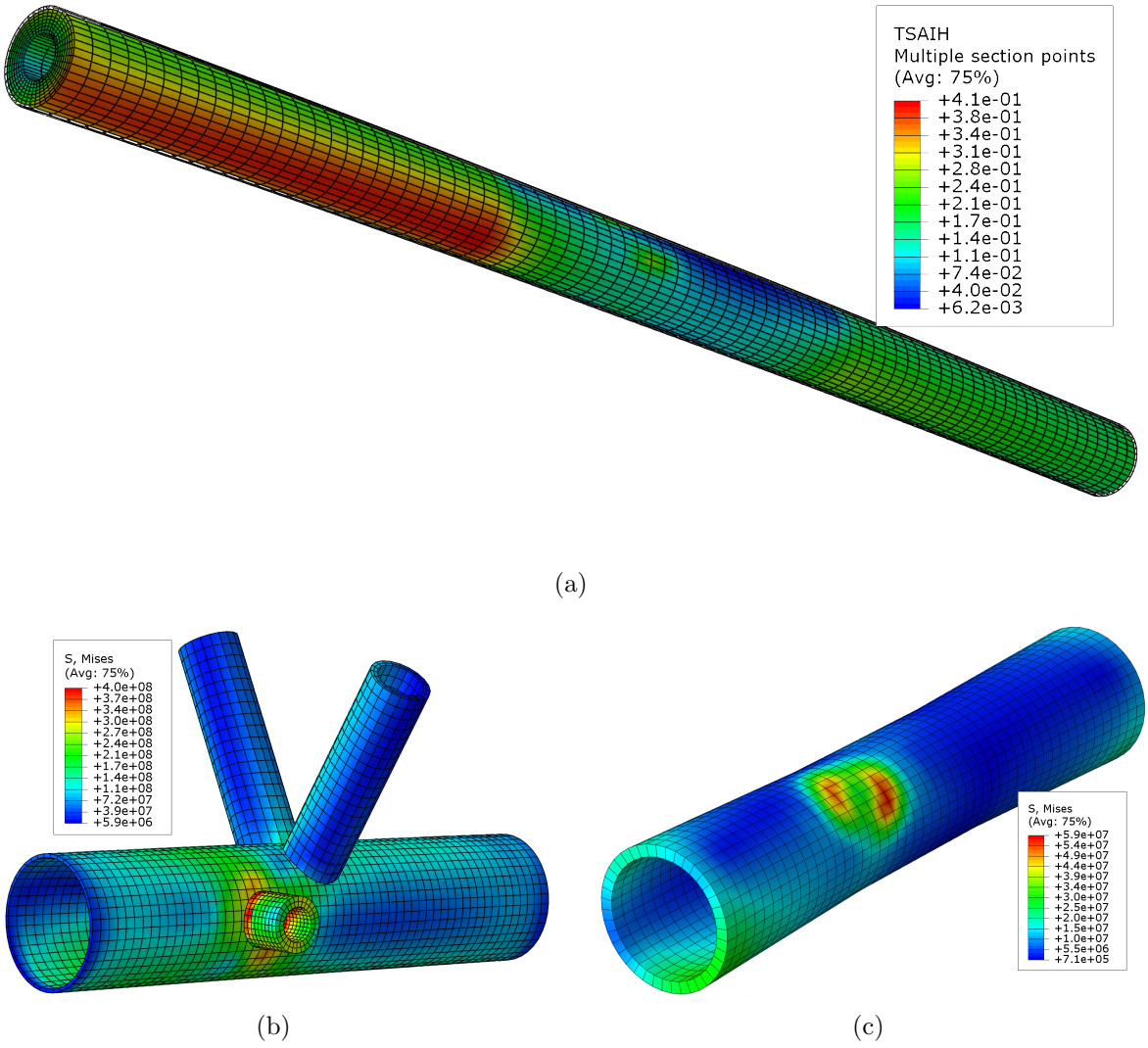

Figure 5.16: *Results with Model 4. (a) Tsai-Hill criterion in blade beam. (b) von Mises stresses in steel. (c) von Mises stresses in adhesive.*

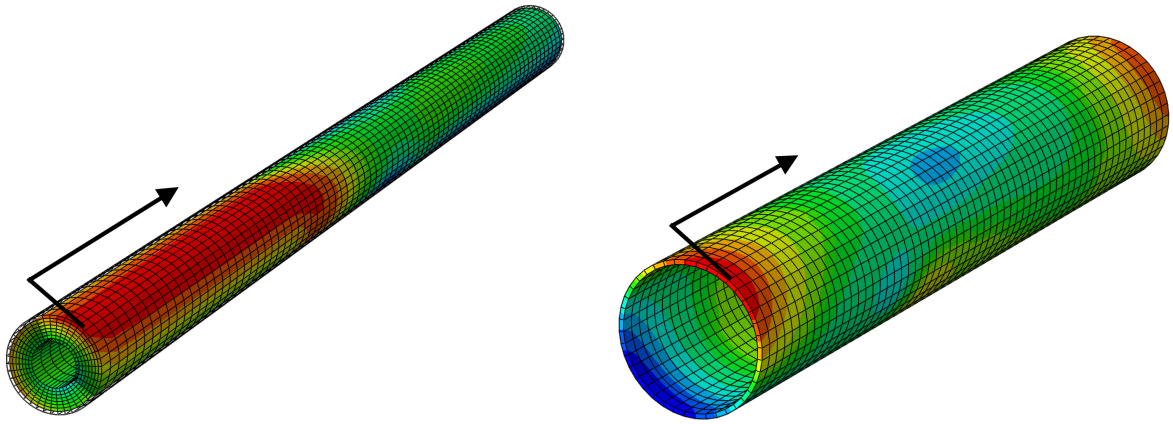

(a)

Figure 5.17: *Illustration of path defined to create plot with results over length. (a) Blade beam. (b) Adhesive layer.*

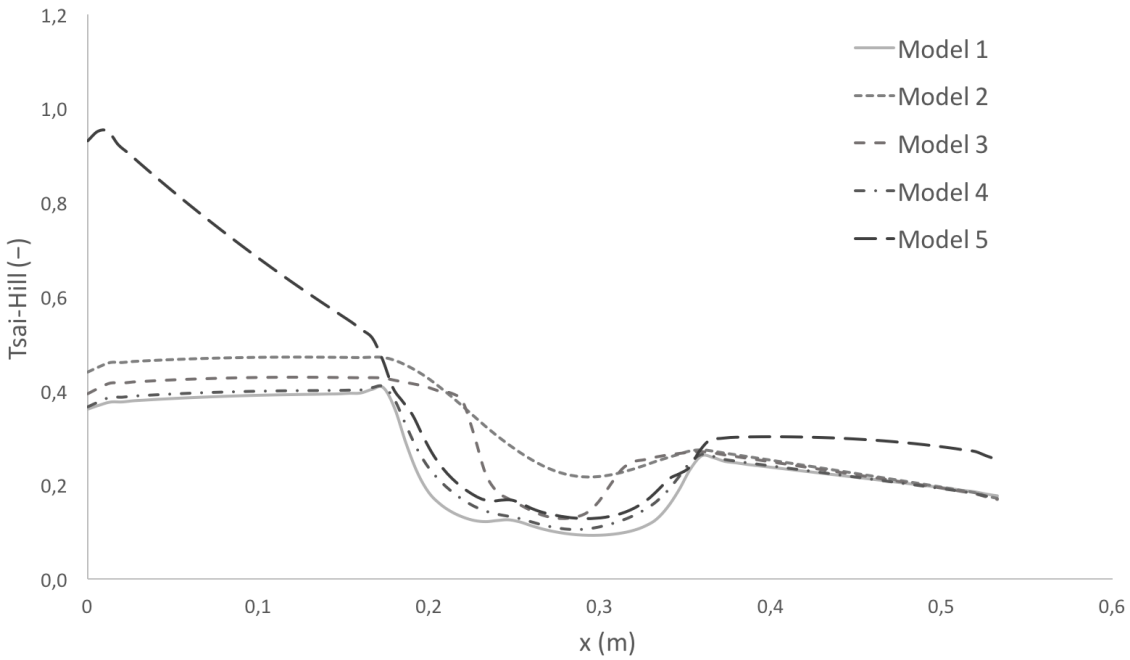

Figure 5.18: *Tsai-Hill criterion in the blade beam over the length, as defined in Figure 5.17, for rotor blade in service.*

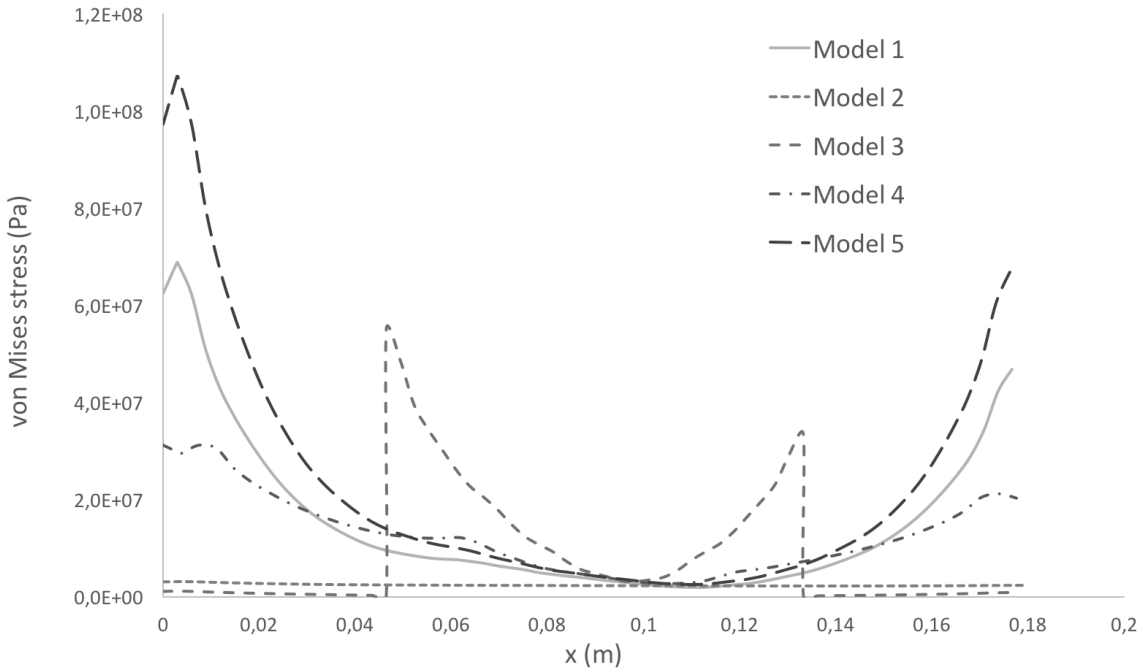

Figure 5.19: *von Mises stress in adhesive over the length, as defined in Figure 5.17, for rotor blade in service.*

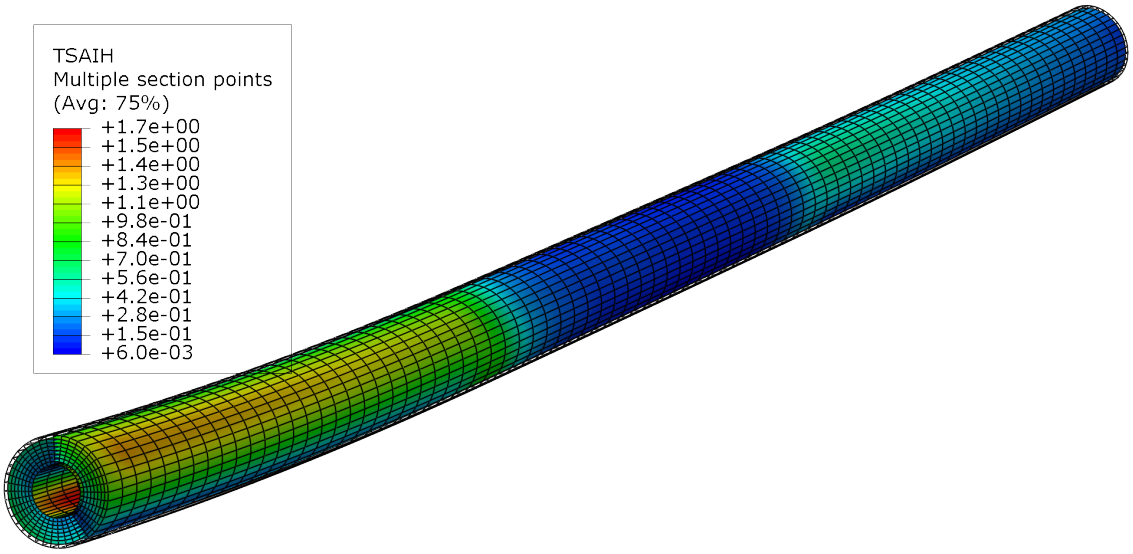

(a)

Figure 5.20: *Results with Model 6 extracted at 50% of the defined load case. Tsai-Hill criterion in blade beam.*

Experimental testing in laboratory

In Figure 5.21 results for Model 8 extracted the moment the Tsai-Hill criterion first exceeds 1.0, i.e. when the blade beam breaks, are presented. The principal appearances of the results from Model 7, 9 and 10 looks similar and the results from Model 8 are included to illustrate the general appearance and stress concentrations.

In Figure 5.22 the magnitude of the concentrated force applied when the Tsai-Hill criterion first exceeds 1.0, i.e. the blade beam fails, are illustrated for model 7 through 10. Furthermore, the diagram also illustrates the share of nodes that have failed in the adhesive layer when the blade beam fails for each model. The adhesive was assumed to fail when the von Mises stress exceeds the shear strength, τ_{max}, of the adhesive, which, according to Table 3.1, is 18.8 MPa for 3M DP490.

5.2.5 Discussion of results

In this section the results from the numerical analyses performed with the design proposal, where a steel section has been introduced is discussed. Initially the results from the numerical analysis for rotor blade in service are discussed. Subsequently, the numerical analyses for experimental testing in laboratory are discussed.

Rotor blade in service

As can be seen in Figure 5.18 and Figure 5.19 the selection of design and materials in the connection element has a significant effect on the results. Model 1 has comparatively low values in Tsai-Hill criterion in the beam. However, the von Mises stresses in the adhesive layer at the end of the lap are untenable. The results when using the soft, deformable, adhesive (Model 2) are good with low and evenly distributed Tsai-Hill criterion and in general low von Mises stresses in the adhesive layer. However, as discussed in Section 3.2.1, SikaFast-5215 NT performance varies remarkably depending on loading speed and temperature. Hence, SikaFast-5215 NT is considered inappropriate. However, since the results is applicable to a similar, soft, adhesive, with highly deformable characteristics the results can turn out to be useful if a similar adhesive, with better properties in terms of permanent loads and temperature variations, is found. The von Mises stresses in Model 3, where the adhesive material changes from the softer to the stiffer adhesive appear to reach infeasible magnitude with clear stress concentrations. These stress concentrations may be reduced by designing the layer with material properties that varies more evenly, e.g. linearly. However, since a solution like this is considered to be hard to construct it was not investigated further.

Designing the adhesive layer with a varying thickness (Model 4) results, as can be seen in Figure 5.19, in comparatively evenly distribution of von Mises stresses over the length in the adhesive layer. Moreover, the distribution and magnitude of Tsai-Hill criterion in the blade beam is similar to the other models with identical design of the blade beam. In Figure 5.18 it appears that an increased diameter of the blade beam closer to the connection (Model 5) results in failure in the beam. Since the cross-section area decreases, higher utilisation rate is of no surprise. However, the fixed boundary condition defined is most likely much stricter than the reality, which could be

a contributing factor to the high values in Tsai-Hill criterion. The results with Model 6, i.e. using a FRC made of glass fibres instead of carbon fibres, suggests that the blade beam fails prior to the load has reached 100%. A modified design of the beam or the composite layup may lead to better results. However, since the results from Model 6 are considered to be far from beneficial this was not investigated further.

Experimental testing in laboratory

As can be seen in Figure 5.21 the stresses are remarkably high and concentrated in the blade beam in the area surrounding the ends of the steel section. Moreover, a large area of the steel has reached yield strength and plastic strains have been developed. Furthermore, the von Mises stress exceeds the shear strength in considerable areas of the adhesive. However, it should be noted that the properties of the FRCs and adhesives are uncertain and it is possible the FRC fails at a lower load or the adhesive can handle higher stresses without failing.

By comparing Model 7 with Model 8 and Model 9 with Model 10 (i.e. the models with constant diameter of the adhesive with the models with varying diameter of the adhesive) in Figure 5.22 it can be seen that the difference appears to be negligible. Hence, for the set up defined for the experimental testing in laboratory varying the thickness of the adhesive layer over the length of the steel section has an insignificant affect on the results. This is in contrast to rotor blade in service, where, as discussed in Section 5.2.5, designing the adhesive layer with varying thickens is beneficial. Moreover, by comparing Model 7 and 8 with Model 9 and 10 (i.e. the models with FRC made of carbon fibres with the models with FRC made of glass fibres) in Figure 5.22 it can easily be seen that the FRC made with carbon fibres fails at notably much higher load than the FRC made with glass fibres. However, the diagram also illustrates that a lower share of the nodes have failed in the adheisve when the blade beam fails when it is made of glass fibres compared to when it is made of carbon fibres. A plausible explanation for this is the substantially much lower force applied when the blade beam fails when it is made of a FRC with glass fibres.

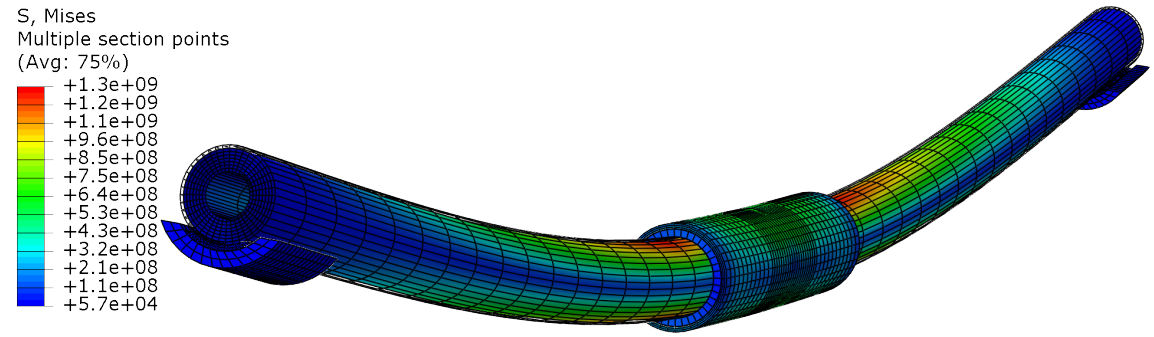

(a)

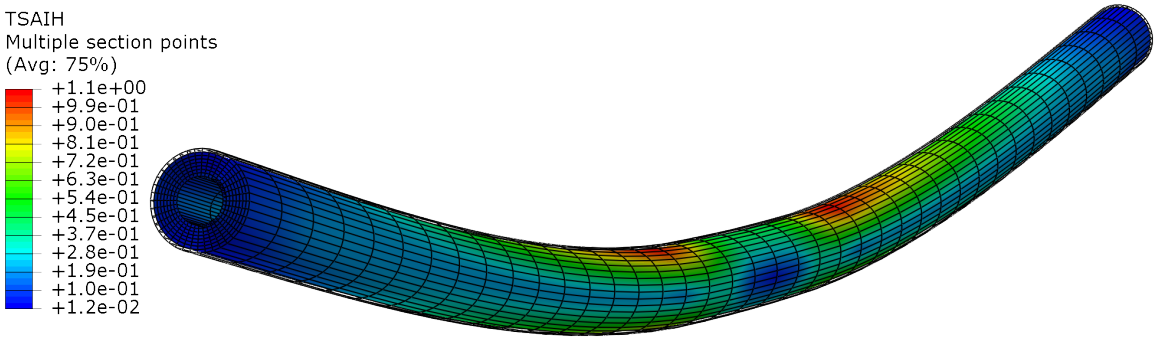

(b)

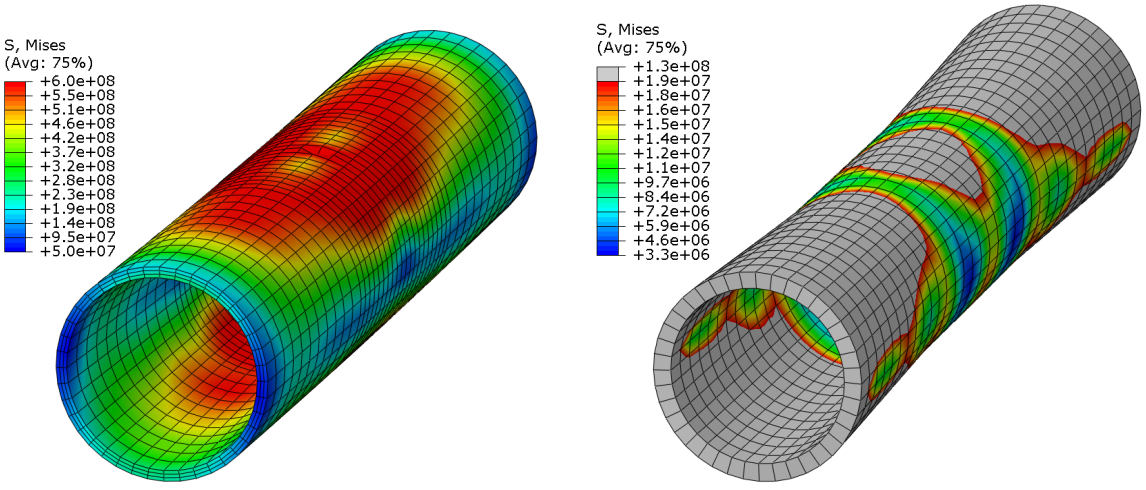

(c) (d)

Figure 5.21: *Results with Model 8. (a) von Mises stresses in assembly. (b) Tsai-Hill criterion in blade beam. (c) von Mises stresses in steel. (d) von Mises stresses in adhesive. The region in grey exceeds the shear strength.*

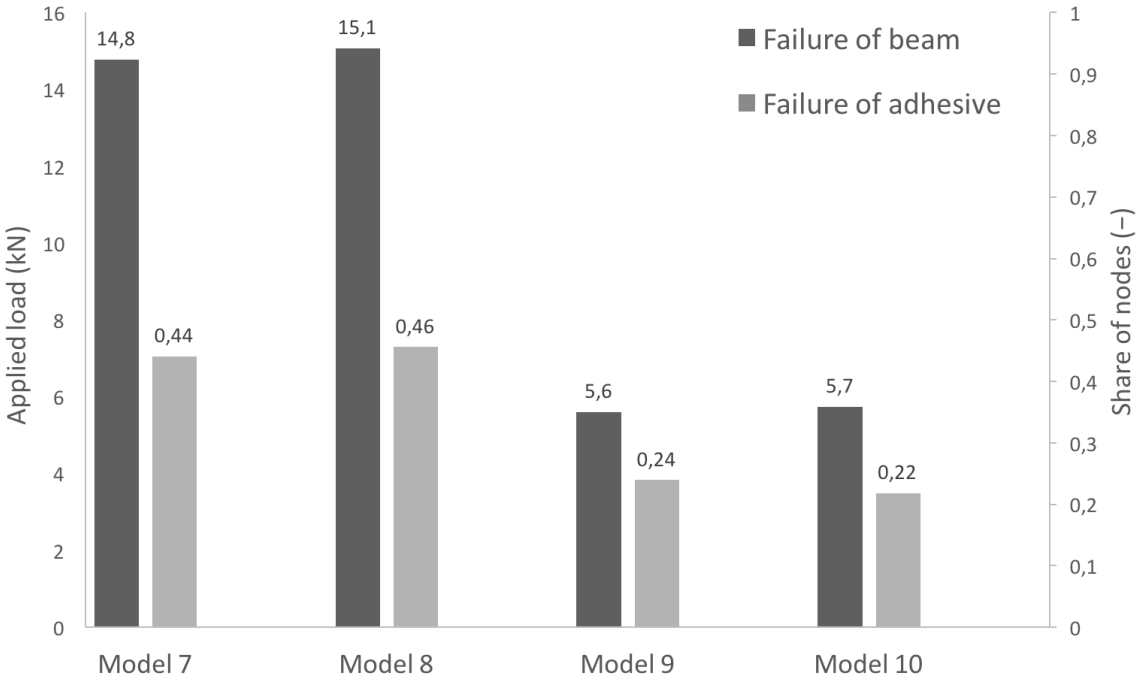

Figure 5.22: *The dark bars are magnitude of concentrated force when blade beam fails according to the vertical axis to the left. The grey bars are share of nodes that have failed in the adhesive layer when the blade beam fails according to the vertical axis to the right.*

6 Concluding remarks

6.1 Conclusions

In the connection element analysed in this work, loads from several structural parts of the rotor blade are transferred. Hence, considering many aspects when designing the element is of significant importance for the further development of the Triblade. Abrupt changes in stiffness, which is the case when elements made of steel are joint with elements made of FRC in the connection element, entails stress concentrations. To reduce the stress concentrations it is beneficial to decrease the stiffness of the stiffer element alternatively increase the stiffness of the less stiff element gradually. Furthermore, a layer of a soft material, e.g. adhesive, between the two elements can be used to reduce stress concentrations.

A design, with all elements connected directly to the blade beam was evaluated in Section 5.1. The abrupt change of stiffness between the steel and FRC induce infeasible stress concentrations. Hence, to reduce the stress concentrations and design the element efficiency, additional structural element must be introduced.

A design, where a steel pipe has been introduced, as presented in Section 5.2, gave substantially much better results. Many parameters affect the way the loads are transferred, e.g. choices of materials, dimensions and shapes of the elements. The element that appears to have the greatest effect is the design of the adhesive. Both the choice of adhesive, where a soft, deformable, adhesive is preferable, and the geometry of the adhesive has a considerable influence on how the loads are transferred. Furthermore, designing the adhesive with a varying thickness over the length of the lap is beneficial.

The blade beam is made of FRCs with either carbon or glass fibres. When the beam is constructed in a FRC with carbon fibres the load at failure is notably much higher than when it is constructed in a FRC with glass fibres. Hence, in a structural perspective a FRC made of carbon fibres is preferable.

Based on the work performed, the connection element should be designed with a steel pipe with the bars and rod-connections welded to it. The blade beam fits into the steel pipe with a thin adhesive layer between, as presented in Section 5.2.2. A soft, highly deformable, adhesive is favourable. Moreover, designing the adhesive with a gradually decreasing stiffness, by either varying the thickness of the layer or the type of adhesive has beneficial effects on the stress distribution in the connection. The blade beam should be made of carbon FRCwith approximately the innermost 10 volumetric percent of the fibres in the $\pm 45°$-direction. The remaining fibres should be oriented in the axial direction of the beam.

6.2 Future work

In the analyses performed simplifications, limitations and assumptions have been made. To fully take all aspects and parameters affecting the connection element and blade beam into account, further research should be conducted. Recommendations for further work includes, but are not limited to:

- Using the set up presented in Section 5.2.3, carry out experimental testing in laboratory to validate the numerical models, find source of errors and for proof-of-concept.
- Dynamic loads, which may be crucial for the connection, were not considered.
- Multiple of the materials used in the connection element have long-term characteristics that should be considered before deciding a final design, e.g. fatigue in the steel and relaxation in the adhesive.
- To determine the most beneficial type of adhesive and FRC to be used in the connection element more detailed studies of the choices of materials are necessary.
- It was shown that a design of the adhesive with a varying stiffness over the length was beneficial for the connection element. In further works a more detailed study of a solution with varying thickness of the adhesive layer, alternatively varying properties of the adhesive material, can be carried out.
- A design of the connection element entirely made of steel has been proposed. However, no analysis of this proposal has been carried out and potential advantages and disadvantages must be considered.
- In Section 3.3.5 a bonded joining technique with protrusions embedded in the FRC was introduced. The effect of this technique in the connection element has not been studied.

Bibliography

[1] R. Gasch and J. Twele, *Wind power plants: fundamentals, design, construction and operation*. Springer, 2 ed., 2002.

[2] E. Hau, *Wind turbines: fundamentals, technologies, application, economics*. Springer, 2 ed., 2006.

[3] F. El-Salem, "Triblade wind turbine," Master's thesis, Energy Sciences, Lund University, 2015.

[4] B. Weddig, "Structural analysis of truss construction for wind turbine blades," Master's thesis, Structural Mechanics, Lund University, 2016.

[5] J. Pettersson, "Analysis and design of an adhesive joint in wind turbine blades," Master's thesis, Structural Mechanics, Lund University, 2016.

[6] "Company," (accessed 2016-11-20). `http://winfoor.com/company/`.

[7] "Technology," (accessed 2016-11-20). `http://winfoor.com/technology/`.

[8] B. Weddig, "Guide to read force diagram generated by fembem." (Unpublished manual), 2016.

[9] B. Weddig and B. Cluzet, "Fembemdyn software." (Unpublished manual), 2016.

[10] E. Kulunk, *Aerodynamics of Wind Turbines*. INTECH Open Access Publisher, 2011.

[11] B. Ästedt, "Stålets egenskaper," 2009-10-12 (accessed 2016-12-05). `http://sbi.se/uploads/source/files/Artiklar/Stalets_egenskaper.pdf`.

[12] B. Sehlå, "Konstruktionsstål," 2009-10-19 (accessed 2016-12-05). `http://sbi.se/uploads/source/files/Artiklar/Konstruktionsstal.pdf`.

[13] B. Burchardt, "Advances in polyurethane structural adhesives," *Advances in Structural Adhesive Bonding*, p. 3565, 2010.

[14] E. Kellar, "Key issues in selecting the right adhesive," *Advances in Structural Adhesive Bonding*, p. 319, 2010.

[15] WoodWisdom-Net, *Load bearing timber-glass composites. Test report on material properties: "WP5: Small Specimen"*, 2012-2014. (Manuscript in preparation).

[16] J. Zangenberg and S. Poulsen, "Glued connecytion in plate shell glass structure," Master's thesis, Section for Structural Engineering, Technical University of Denmark, 2010.

[17] P. K. Mallick, *Fiber-reinforced composites: materials, manufacturing, and design*. CRC Press, 3 ed., 2008.

[18] "Mechanical properties," (accessed 2017-01-06). `http://www.performance-composites.com/carbonfibre/mechanicalproperties_2.asp`.

[19] K. Dilger, "Selecting the right joint design and fabrication techniques," *Advances in Structural Adhesive Bonding*, p. 295315, 2010.

[20] P. A. Ciullo and N. Hewitt, *The rubber formulary*. Noyes Publications, 1999.

[21] N. S. Ottosen and H. Petersson, *Introduction to the finite element method*. Prentice Hall, 1992.

[22] Dassault Systémes SIMULIA., *Abaqus/CAE User's Guide (6.14)*.

[23] S. Heyden, O. Dahlblom, A. Olsson, and G. Sandberg, *Introduktion till strukturmekaniken*. Studentlitteratur, 2008.

[24] PLAXIS, *PLAXIS Version 8 Material Models Manual*.

[25] "Von mises stress," (accessed 2016-11-05). `http://www.continuummechanics.org/vonmisesstress.html`.

[26] A. J. Kolios and S. Proia, "Evaluation of the reliability performance of failure criteria for composite structures," *World Journal of Mechanics*, vol. 02, no. 03, pp. 162–170, 2012.

[27] M. Davis and D. Bond, "The importance of failure mode identification in adhesive bonded aircraft structures and repairs," *The International Conference on Composite Materials ICCM-12*, July 1999.

A Forces in connection element

Following contents are presented in this appendix:

Figure A.1: *Locations and coordinate systems of the forces given in Table A.1. The normal forces in Rod 1 and Rod 6 are oriented parallel to the corresponding rod. The coordinate system illustrated in the centre of the beam is the local coordinate system for Blade 2-1 and Blade 2-2.*

Table A.1: *Internal forces in the connection element analysed when subjected to the worst load case. The rods are modelled as wires, hence only axial forces are present in these [8].*

	Blade 2-1	Blade 2-2	Bar 2-1	Bar 2-2	Rod 1	Rod 6
Normal Force (N)	-42,950	-25,720	4,034	-2,271	12,450	6,013
Shear force, Y-direction (N)	-123.6	-139.2	71.31	-72.74		
Shear force, Z-direction (N)	-587.5	327.2	-55.82	-21.43		
Torque (Nm)	13.1	54.4	0.60	-0.55		
Bending moment about Y-axis (Nm)	-256.2	-256.2	-15	6.68		
Bending moment about Z-axis (Nm)	-108.2	-108.2	-15.87	-24.59		

B SikaFast-5215 NT

Following contents are presented in this appendix:

B.1 Product data sheet

Industry

Produktdatablad
Version 1 (05/2013) 2013-07-22
SikaFast®-5215 NT

SikaFast®-5215 NT

Snabbhärdande tvåkomponents strukturlim

Tekniska data

Egenskaper		Komponent A SikaFast®-5215 NT	Komponent B SikaFast®-5200
Kemisk bas		Akryl	
Färg (CQP[1] 001-1)		Vit	Svart
Färg blandad		Grå	
Härdningsmekanism		Radikal polymerisation	
Densitet (CQP 006-4)		Ca 1,15 kg/l	Ca 1,5 kg/l
Densitet blandad (beräknad)		Ca 1,19 kg/l	
Blandningsförhållande	efter volym	10 : 1	
	efter vikt	10 : 1,3	
Konsistens		Tixotrop pasta	
Appliceringstemperatur		5 - 40°C	
Öppentid[2] (CQP 526-2)		Ca 5 min	
Fixeringstid[2]	tid för att nå 80% av slutstyrkan	Ca 15 min	
Hårdhet Shore A (CQP 023-1 / ISO 868)		Ca 90	
Hårdhet Shore D (CQP 023-1 / ISO 868)		Ca 50	
Draghållfasthet[2] (CQP 036-1 / ISO 37)		Ca 10 MPa	
Brottöjning[2] (CQP 036-1 / ISO 37)		Ca 200%	
E-Modul[2] (CQP 036-1 / ISO 37)		Ca 250 MPa	
Skjuvhållfasthet[2] (CQP 046-6 / ISO 4587)		Ca 10 MPa	
Glastransitionstemperatur (CQP 509-1 / ISO 6721-2)		Ca 60°C	
Servicetemperatur		-40 - 80°C	
Hållbarhet[3] (CQP 016-1)	Patron 50 ml	15 månader	
	Patron, övriga	9 månader	
	Hink / Fat	12 månader	9 månader

[1] CQP = Corporate Quality Procedures [2] 23°C / 50% r.h. [3] Lagrad under 25°C och ej exponerad till direkt solljus

Beskrivning

SikaFast®-5215 NT är ett snabbhärdande, flexibelt, tvåkomponents strukturlimsystem vilket är baserat på Sikas Acrylic Double Performance (ADP) polymerteknologi.
Ohärdad SikaFast®-5215 NT är ett pastöst, tixotropt, svårantändligt material som tillåter en enkel och precis applicering.
SikaFast®-5215 NT produceras i enlighet med kvalitetssäkrings- respektive miljöledningssystem certifierade enligt ISO 9001/14001 och enligt Ansvar & Omsorgsprogrammet.

Produktfördelar

- Styrkeuppbyggnad inom minuter efter applicering
- Vidhäftning till ett brett spektrum av material utan eller med begränsad förbehandling
- Hög styrka och slagtålighet
- Lösningsmedel- och syrafri
- Mindre lukt än produkter innehållande MMA
- Enkel att blanda

Applikationsområden

SikaFast®-5215 NT är ett snabbhärdande, flexibelt strukturellt lim framtaget för att ersätta mekaniska fästelement som nitar, skruvar och svetsning. Den är lämplig till höghållfasta dolda förband och har utmärkt vidhäftning till olika material inklusive topplacker, plaster, glas, trä, etc.
Denna produkt skall endast användas av erfarna användare. Förprov skall utföras på aktuella underlag och vid rätt förhållanden för att säkerställa vidhäftning och kompabilitet mellan materialen.

Härdmekanism

SikaFast®-5215 NT härdar genom radikal kedjepolymerisering när den blandas med SikaFast®-5200. Öppen- och fixeringstiden påverkas av variationer i blandningsförhållandet och temperaturen, d.v.s. högre temperatur ger kortare öppen- och fixeringstid och tvärtom.

Kemisk resistens

SikaFast®-5215 NT är resistent mot många kemikalier. För specifik information, kontakta den tekniska avdelningen hos Sika Industry.

Vidhäftningsresultat

Följande tabell sammanfattar skjuvprovningsresultat erhållna med olika sorters standardsubstrat. Dessa resultat är endast en indikation. På grund av mångfalden av substrat måste preliminära prov utföras.

Adhesiontabell (typiska värden)

Material	BM[1]	Värde
AlMg3	K	10 MPa
Rostfritt stål	K/A	8 MPa
El. galv. stål	K/A	10 MPa
Glas	K/A	9 MPa
ABS	S	8 MPa
PVC	K	10 MPa
PC	K	10 MPa

Tabell 1: Skjuvförband enl. ISO 4587 Limtjocklek 1.5 mm

[1] *Brott mod: **A**dhesivt, **K**ohesivt, **S**ubstrat*

Appliceringsmetod

Förbehandling

Ytorna som ska limmas måste vara rena torra och fria från alla spår av fett, olja och damm. Avlägsna alla lösa partiklar och rester genom noggrann rengöring. För bästa vidhäftnings-egenskaper förbehandla limytorna med Sika® ADPrep innan limprocessen. På grund av mångfalden av material är det nödvändigt att göra förprov med material av produktions-kvalité. Applikationsspecifik rådgivning finns tillgänglig hos Teknisk Service.

Applicering

SikaFast®-5215 NT appliceras i ett blandningsförhållande på 10:1 (volym) (± 10%) genom en 24 elements statisk mixer.
Tänk på att om limmet appliceras i stora mängder bildas värme genom den exoterma reaktionen. För att undvika höga temperaturökningar skall limtjockleken vara maximalt 3 mm men måste dock vara minst 0,5 mm. Det blandade limmet har en öppentid på ca 5 minuter och uppnår hanteringsstyrka (fixeringstid) på ca 15 minuter. Optimal temperatur för limprocessen är mellan 15°C och 25°C. Det godkända temperaturintervallet för substrat och lim är mellan 5°C and 40°C. Reaktivitetens påverkan av temperaturändringar måste respekteras.
Efter öppentidens utgång får inte de limmade detaljerna flyttas relativt varandra. När fixeringstiden är nådd kan detaljerna flyttas om ingen ytterligare kraft påverkar fogen.
För ytterligare information och support vid utvärdering av lämplig appliceringsutrustning var god kontakta Sikas systemavdelning hos Sika Industry.

Rengöring

Ohärdad SikaFast®-5215 NT kan avlägsnas med Sika® Remover-208 eller annat lämpligt lösningsmedel. Härdat material kan endast avlägsnas mekaniskt.
Händer och hud som nedsmutsats tvättas omedelbart med Sika® Handclean eller annat lämpligt tvättmedel för industriellt bruk. Använd aldrig lösningsmedel!

Övrig Information

Följande information finns tillgänglig på begäran:
- Säkerhetsdatablad
- Generella riktlinjer för limning med SikaFast® lim

Förpackningsinformation

Dubbelpatron	50 ml
Dubbelpatron	250 ml
Hink SikaFast®-5215 NT	20 l
Hink SikaFast®-5200	18 l
Fat SikaFast®-5215 NT	169 l

Underlag för tekniska data

Alla tekniska värden som anges i detta produktdatablad är baserade på laboratorie-tester. Aktuella mätta värden kan variera på grund av faktorer utanför vår kontroll.

Viktigt

För information och råd om säker hantering, lagring och avfallshantering av kemiska produkter hänvisas användaren till gällande säkerhetsdatablad vilket innehåller fysisk, ekologisk, toxikologisk och annan säkerhetsrelaterad information.

Lagstiftning

Informationen, och i synnerhet, rekommendationerna avseende appliceringen och användandet av Sika produkter, ges i god tro baserat på Sikas rådande kunskap och erfarenhet av produkterna när de lagrats, hanterats och applicerats på korrekt sätt under normala förhållanden. I praktiken är skillnaden hos material, substrat och verkliga platsförhållande sådana att ingen garanti avseende kurans eller lämplighet för ett speciellt användningsområde kan lämnas. Med hänsyn härtill kan något rättsligt ansvar av vad slag det må vara varken härledas från denna information eller från någon skriftlig rekommendation eller i övrigt beträffande produkten lämnade råd. Användaren av produkten måste prova produktens lämplighet för den tilltänkta applikationen och syftet. Sika reserverar sig för rätten att ändra sina produkters egenskaper. Hänsyn måste vid användningen även tas till tredje mans ägande och andra eventuella rättigheter. Alla beställningar accepteras med förbehåll för våra gällande allmänna försäljnings- och leveransvillkor. Användaren måste alltid rådfråga senaste gällande utgåva av det lokala produktdatabladet för produkten ifråga. Kopior av detta finns tillgänglig på begäran.

Mer information tillgänglig på:
www.sika.se
www.sika.com

Sika Sverige AB
Industriavdelningen
Domnarvsgatan 15
SE-163 08 Spånga
Sverige
Tel. +46 (0)8 621 89 00
Fax +46 (0)8 621 89 89

B.2 Lap shear test

Sika Technology AG
polymer testing lab **05.06.2012**

Kunde	: Sabrina Kirchhofer	Prüfgeschwindigkeit	: 10 mm/min
Prüfer	: Tanja Kordic	Prüfverfahren	: Zugscherversuch
Prüfnorm	: EN 1465 - CQP046-6	Versuchsart	: Zugversuch
Prüfdatum	: 05.06.2012	Prüfklima	: 23±1°C / 50±5% rel.Feuchte
Vorkraft	: 1 N		
Klebstoff	: Fast 5215 NT ADP AlMg3 1dRT (ZSF)		
Bemerkungen	:		

Ergebnisse:

Legende	Nr	Breite mm	Lü mm	τ MPa	Fmax N
———	1	25	11.7	11.35	3321.3
—— ——	2	25	11.6	10.99	3186.9
- - - - - - -	3	25	11.7	11.77	3442.0

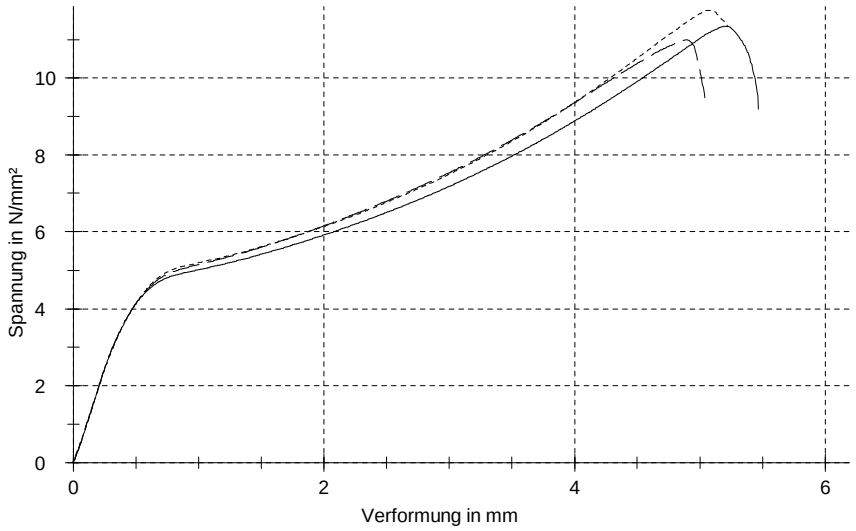

Statistik:

Serie n = 3	τ MPa	Fmax N
$\bar{x}$	11.37	3316.7
s	0.39	127.6

C Drawings

Following contents, created by Winfoor, are presented in this appendix:

C.1	**Steel section, rod-connections and bars**	Drawings with dimensions of steel section, rod-connections and bars.
C.2	**Blade beam**	Drawings with dimensions of blade beam.
C.3	**Angles**	Drawings with angles.

C.1 Steel section, rod-connections and bars

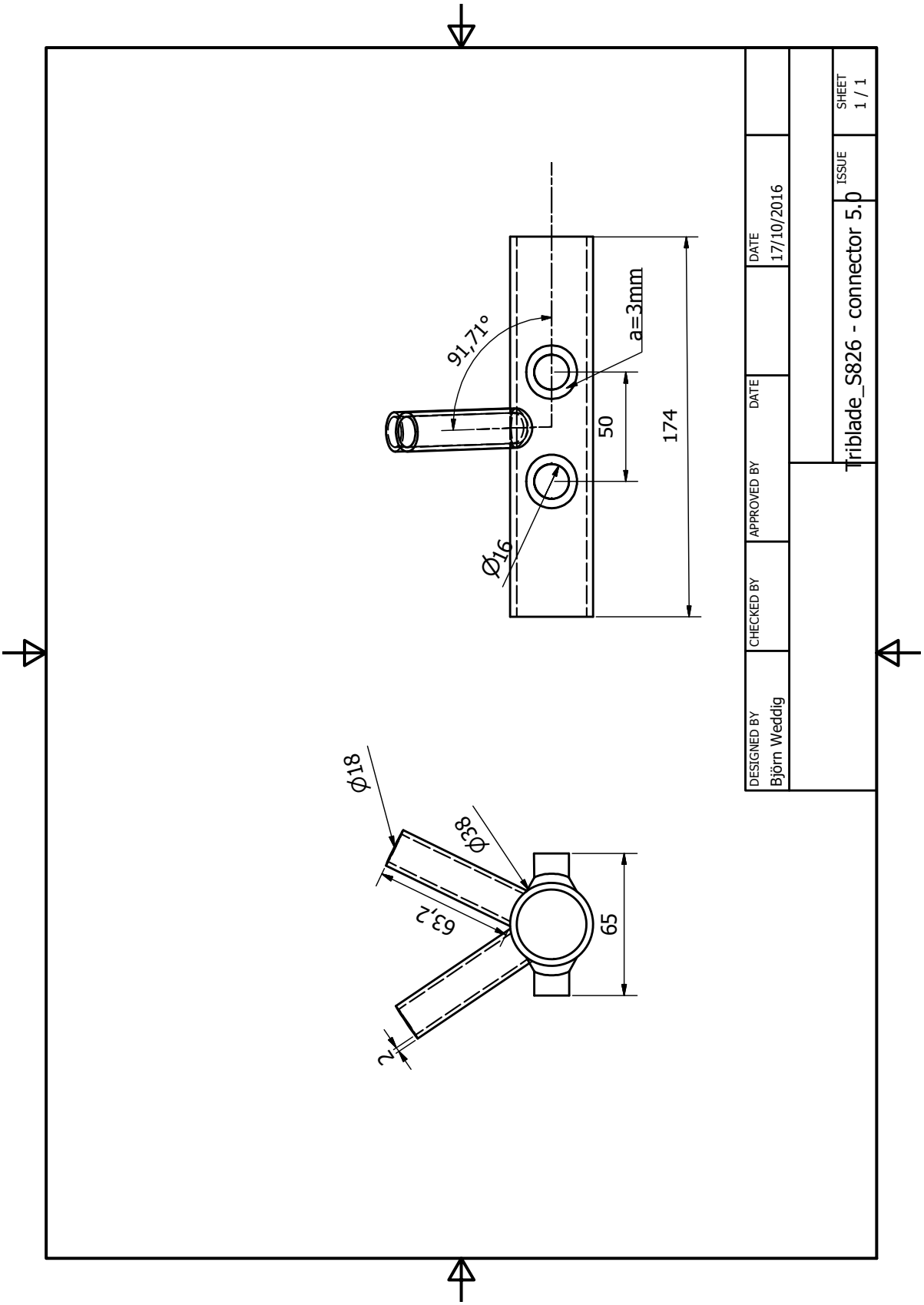

C.2 Blade beam

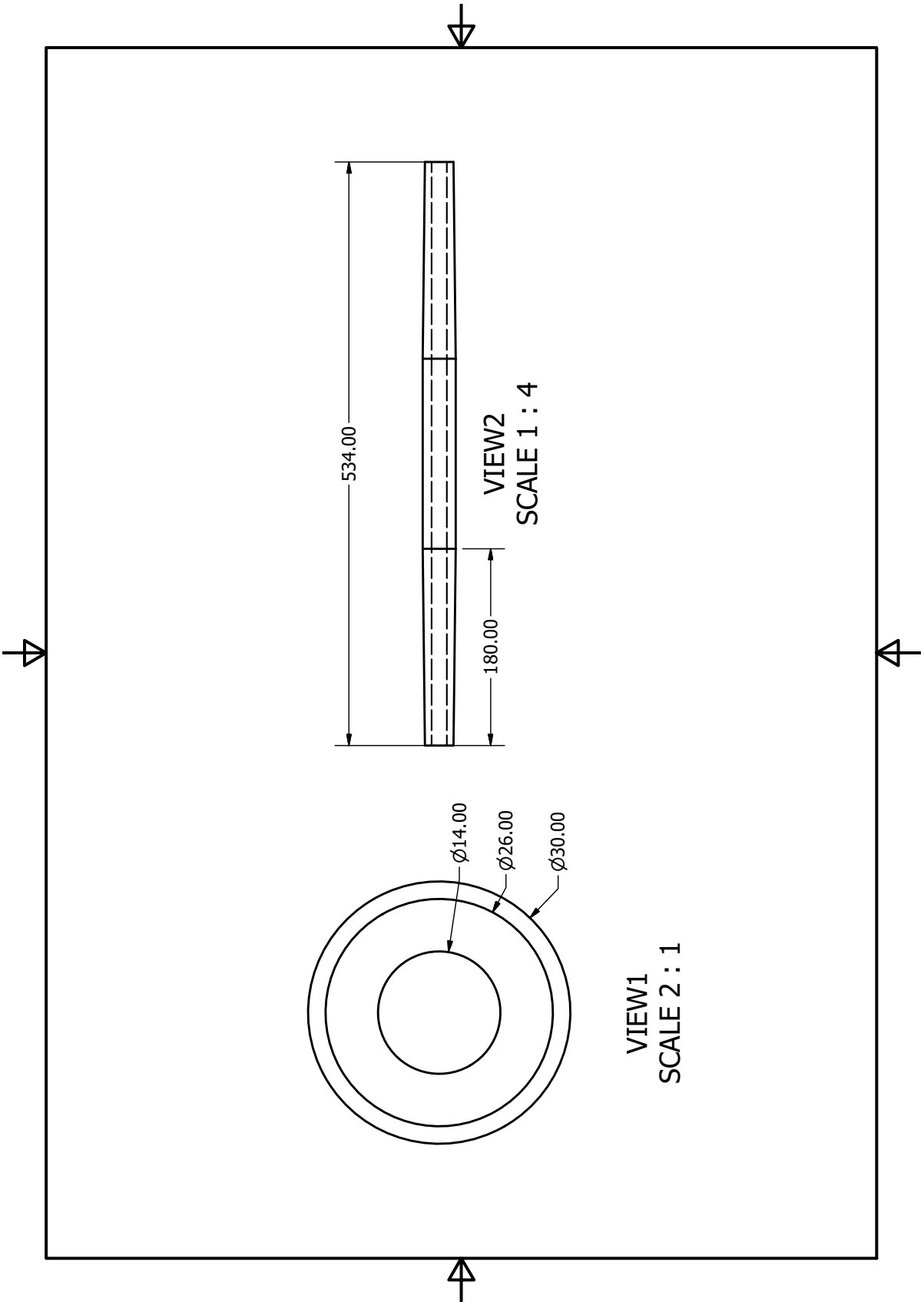

C.3 Angles